Mineralium Deposita (2020) 55:491–513
https://doi.org/10.1007/s00126-019-00893-5

ARTICLE

Sources and ore-forming fluid pathways of carbonate-hosted Pb–Zn deposits in Southwest China: implications of Pb–Zn–S–Cd isotopic compositions

Chong Xu[1,2] · Hong Zhong[1,2] · Rui-Zhong Hu[1,2] · Han-Jie Wen[1,2] · Wei-Guang Zhu[1] · Zhong-Jie Bai[1] · Hai-Feng Fan[1] · Fang-Fang Li[1] · Ting Zhou[1]

Received: 23 July 2018 / Accepted: 1 May 2019 / Published online: 27 May 2019

Abstract

The Sichuan–Yunnan–Guizhou metallogenic province of Southwest China contains more than 200 Mt of Pb–Zn ore in carbonate-hosted Pb–Zn deposits, representing ~ 27% of the total Pb and Zn resources of China. Sources of metals and pathways of ore-forming fluids were elucidated through a study of the Pb–Zn–S–Cd isotopic compositions of sphalerite from the Tianbaoshan, Fusheng, Maozu, Jinshachang, and Daliangzi carbonate-hosted Pb–Zn deposits. $\delta^{34}S$ values indicate that S in the deposits is derived mainly from evaporites in Cambrian to Triassic sedimentary strata, sulfates coexisting with sulfides, and Meso–Neoproterozoic folded basement. $\delta^{66}Zn$ values and Pb isotopic ratios indicate that these metals originate mainly from Sinian to lower Permian sedimentary rocks and Proterozoic basement. There is a trend towards isotopically heavier Cd and Zn compositions of sphalerite from Maozu to Daliangzi, Jinshachang, and Tianbaoshan, which are all hosted in the upper Sinian Dengying Formation. Previous studies showed that there would be a trend of enrichment in heavier Zn and Cd isotopes following the migration of fluids and precipitation of minerals. The above observations suggest that the ore-forming fluids of these deposits are probably derived from the same hydrothermal fluid system. The fluids most likely flowed through Maozu first, migrating along the Xiaojiang and Anninghe fault belts and their branch faults to Daliangzi, Jinshachang, and Tianbaoshan, respectively. Zn and Cd isotopes could be useful tools in tracing the pathways of ore-forming fluids in this district, and heavier Zn and Cd isotopic compositions could provide a geochemical fingerprint for detecting remote orebodies in large hydrothermal fluid systems.

Keywords Carbonate-hosted Pb–Zn deposit · Pb–Zn–S–Cd isotopes · Metal sources · Ore-forming fluid pathways · Southwest China

Introduction

The Sichuan–Yunnan–Guizhou ("SYG triangle") Pb–Zn metallogenic province in the western Yangtze Block of Southwest China contains more than 400 Pb–Zn deposits, with ~ 200 Mt of Pb–Zn ore having average Pb and Zn grades of 5 wt% and 10 wt%, respectively. Resources identified in this area represent ~ 27% of the total Pb and Zn resources of China (Zhang et al. 2013; Zhou et al. 2014b). The deposits are hosted in Sinian to Permian carbonate rocks, structurally controlled by thrust faults and folds, and spatially associated with ~ 260 Ma Emeishan flood basalts (Zhou et al. 2002, 2014b). Many Pb–Zn deposits in the area are known for extreme enrichment in trace elements, such as the Huize Ge-rich (Fu 2004; Han et al. 2012; Ye et al. 2011; Wu 2013; Zhu 2014), Fule Cd-rich (Si 2005; Zhu et al. 2013, 2017; Zhu 2014), and Tianbaoshan Cd-rich (Fu 2004; Zhu 2014) deposits. To better constrain their origins and to trace their metal sources, various deposit types have been proposed on the basis of their geology and geochemistry including, for

Editorial handling: B. Lehmann

Electronic supplementary material The online version of this article (https://doi.org/10.1007/s00126-019-00893-5) contains supplementary material, which is available to authorized users.

✉ Hong Zhong
zhonghong@vip.gyig.ac.cn

[1] State Key Laboratory of Ore Deposit Geochemistry, Institute of Geochemistry, Chinese Academy of Sciences, Guiyang 550081, China

[2] University of Chinese Academy of Sciences, Beijing 100049, China

example, results of fluid inclusion and C–H–O–S–Pb isotopic studies (Xie 1963; Huang et al. 2003, 2004; Li 2003; Li et al. 2007; Zhu et al. 2013; Zhang et al. 2015). "Magmatic hydrothermal" (Xie 1941, 1963), "sedimentary reworking" (Tu 1984; Zhang 1984; Chen 1986; Zhao 1995; Liu and Lin 1999), and the most representative MVT (Zhou et al. 2001; Zhang et al. 2007; Han et al. 2007a; Hu and Zhou 2012; Wu et al. 2013) deposits have previously been described.

Sulfur and Pb isotopes have long been used to trace metal sources and constrain origins of Pb–Zn deposits. Lead isotopic studies have indicated that metals in the SYG Pb–Zn deposits are sourced from Precambrian basement and/or Paleozoic host rocks (e.g., Zhou et al. 2001; Zhou et al. 2013a, b, c, 2014a, b), while S isotopic studies have indicated that reduced S was produced by thermochemical sulfate reduction (TSR) of evaporites in host strata (e.g., Han et al. 2007a; Zhou et al. 2014a, b). Liu et al. (2017) considered that S in the SYG deposits was produced from sulfates in the Youjiang Basin where a thermal anomaly of 200–350 °C developed during the Middle Triassic. This anomaly may have caused TSR, reducing aqueous sulfate in basin brine. Recent studies indicate that stable Cd and Zn isotopes have potential in elucidating ore formation processes (Kelley et al. 2009; Zhu et al. 2013; Wen et al. 2016). Zhu et al. (2013) found that the various types of Pb–Zn deposits have characteristic Cd contents and isotopic compositions, and Wen et al. (2016) postulated that Cd isotopic compositions could be an effective indicator of ore formation processes and deposit classification. Previous studies have also shown that during the evolution of fluids from early to late stages, residual fluids and late-stage sulfide precipitates exhibit heavier Zn isotopic compositions than those precipitated earlier (Mason et al. 2005; Wilkinson et al. 2005; John et al. 2008; Sivry et al. 2008; Kelley et al. 2009; Dekov et al. 2010; Zhou et al. 2014a, b). There are also significant differences in Zn isotopic compositions among various crustal sources. For example, the average δ^{66}Zn values for silicate Earth and deep seawater are 0.28‰ ± 0.05‰ (Chen et al. 2013) and ~ 0.50‰ (Little et al. 2014; Zhao et al. 2014), respectively, while δ^{66}Zn values of marine carbonate can isotopically heavier up to ~ 1.3‰ (Pichat et al. 2003; Kunzmann et al. 2013), with such differences indicating a potential for Zn isotopes in tracing sources of the metal. These studies suggested that different stratigraphic units could exhibit similar or different Zn isotopic compositions, and leaching and concentration of Zn in fluid during migrating through the host-rock sequence could also change their isotopic compositions. This provides a possibility utilizing Zn isotopes to demonstrate the sources and pathways of ore-forming fluids for the Pb-Zn deposits.

However, there is a lack of systematic and comparative studies of the SYG Pb–Zn metallogenic province, especially for non-traditional isotopes such as Zn and Cd, and the metal sources remain controversial. The present study aimed to elucidate metal sources and the pathways of their ore-forming fluids. Sphalerite separates from five representative carbonate-hosted Pb–Zn deposits within different stratigraphic sequences, namely the Tianbaoshan, Fusheng, Maozu, Jinshachang, and Daliangzi deposits in the southwestern part of the SYG Pb–Zn metallogenic province, were selected for systematic Pb–Zn–S–Cd isotopic study (Fig. 1a).

Geological background

Geological setting

The SYG triangle, on the southwestern margin of the Yangtze Block (Fig. 1b), covers an area of ~ 170,000 km^2 within northeastern Yunnan Province, northwestern Guizhou Province, and southwestern Sichuan Province (Hu et al. 2016). The triangle is confined by three regional fault belts extending deep into basement rocks: the N–S-trending Anninghe, NE–SW-trending Mile–Shizong, and NW–SE-trending Weining–Shuicheng fault belts. It also contains the deep-seated N–S-trending Xiaojiang fault belt (Fig. 1a). These long-lived fault belts have been activated and reactivated by a number of tectonic events and may have acted as conduits for Emeishan basalts and hydrothermal fluids (Zhang 2008). The area also contains numerous secondary NE–SW- and NW–SE-trending faults and fold-and-thrust belts (Fig. 1a).

The stratigraphy of the SYG triangle includes pre-Sinian basement, Sinian to lower Mesozoic submarine sedimentary sequences, and Jurassic to Cenozoic terrigenous sediments. The crystalline basement of the Yangtze Block is thought to consist of Archean (3.3–2.9 Ga) metamorphic rocks (Qiu et al. 2000; Gao et al. 2011). The late Paleoproterozoic to early Mesoproterozoic Dongchuan (1.7–1.5 Ga) and Mesoproterozoic Kunyang (1.2–0.9 Ga) groups are widely distributed throughout the study area and are dominated by siltstones, slates, sandstones, and dolostones interbedded with tuffaceous units (Zhao et al. 2010; Hu et al. 2017a, b). These rocks form the basement, which is tightly folded but only weakly metamorphosed (Zhou et al. 2013b).

The southwestern Yangtze Block was a passive continental margin during the Sinian to Middle Triassic, leading to deposition of thick submarine sedimentary sequences that cover the basement rocks and are dominated by carbonates and clastic sediments (Wu et al. 2013). The lower Sinian units are dominantly coarse volcaniclastic sediments, while the uppermost unit is a thick dolostone layer. Cambrian rocks are dominantly clastic sediments and include black shales, sandstones interlayered with dolostones, and

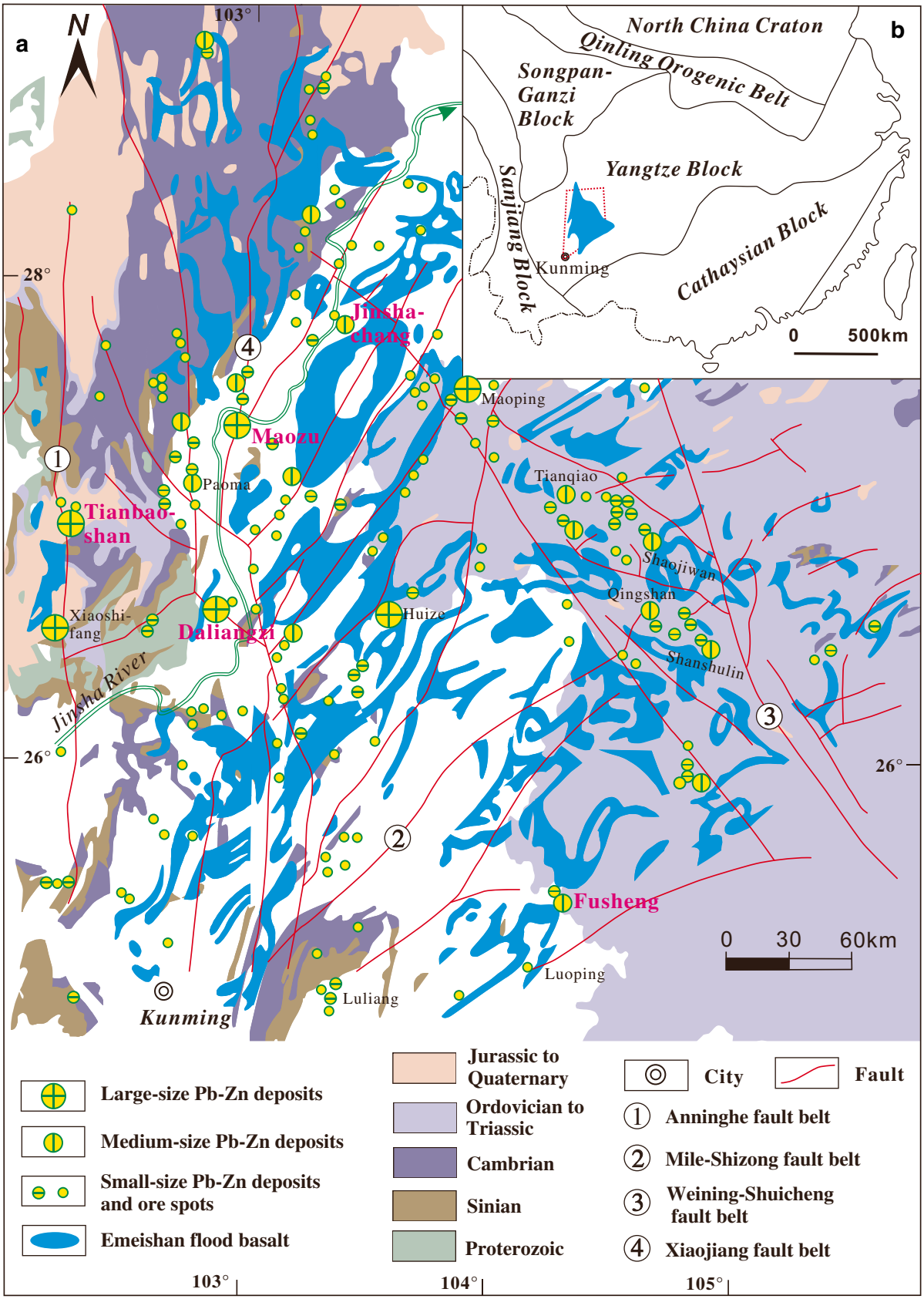

Fig. 1 (**a**) Simplified geological map of the Sichuan-Yunnan-Guizhou MVT triangle (after Zhang et al. 2015; Zhu et al. 2016). (**b**) Simplified tectonic map of South China (after Zhu et al. 2016)

limestones. Ordovician sediments are dominantly limestones, dolostones, marls, and shales. Silurian sediments are dominated by fine-grained sandstones, shales, dolostones, and limestones. Devonian sediments are dominated by quartz sandstones, calcareous sandstones, shales, limestones, dolomitic limestones, and dolostones, all of which are overlain by Carboniferous limestones, oolitic limestones, dolomitic limestones, and dolostones. Lower Permian sediments include microcrystalline limestones, brecciated limestones, dolomitic limestones, dolostones, and argillaceous siltstones, overlain by voluminous Permian Emeishan flood basalts erupted and emplaced at 263–251 Ma (Zhong and Zhu 2006; He et al. 2007; Xu et al. 2008). The closure of the Paleo-Tethys Ocean was followed by tectonism related to the Indosinian Orogeny and post-Late Triassic completion of suturing between the Indochina and South China blocks around the study area (Cai and Zhang 2009). This led to the development of a series of thrust belts and foreland basins on the periphery of the region. The SYG triangle was also affected by subsequent continuous intracontinental deformation and the deposition of terrigenous sandstones, conglomerates, and freshwater marls of Jurassic to Cenozoic age (Wu et al. 2013).

The Tianbaoshan deposit

The Tianbaoshan Pb–Zn deposit is hosted in Sinian carbonate rocks and is structurally controlled by the N–S-trending Anninghe fault belt and its branch structures (Fig. 1a). In the Tianbaoshan ore district, the Sinian stratum represents the upper Sinian Dengying Formation, comprising mainly dolostone. The overlying middle Cambrian Xiwangmiao Formation is dominated by clastic rocks and black shales, while the Upper Triassic Baiguowan Formation is composed of continental sandstone and shale. NW–SE- and NNW–SSE-trending faults and NE–SW-trending folds are intensively developed in the ore district (Fig. 2a). The main folds are the Tianbaoshan syncline and its secondary synclines and anticlines (e.g., Xinshangou, Shagou synclines and anticlines; Fig. 2a). In the ore field, diabase dikes occur in the N–S- and NW–SE-trending faults and usually cut the orebodies.

Major orebodies occur in dolostone of the upper Sinian Dengying Formation and are structurally controlled by concealed NW–SE-trending fractures (Fig. 2a). Underground mining and exploratory drilling provide excellent access to two ore sections (Tianbao and Xinshan) and three orebodies. The largest orebody is in the Tianbao section and is 400 m deep, 285 m long, and 2–50 m wide. Ores in this body contain 1.8 Mt Pb–Zn with grades of 1.3–2.5 wt% Pb, 7.8–10.1 wt% Zn, and 96.3 g t^{-1} Ag (Wang et al. 2000). The ores also contain small amounts of Ge, Ga, and Cd (Fu 2004) thought to be hosted in sphalerite and galena (Zhou et al. 2011). The orebodies are stratabound as tabular, lenticular, and vertical pipe forms with sharp boundaries with host rocks.

The Pb–Zn ores are predominately sulfides, with small amounts of oxidized ores. Ore minerals include sphalerite, galena, pyrite, chalcopyrite, arsenopyrite, freibergite, and pyrargyrite, with calcite, dolomite, and quartz as gangue minerals (Fig. 4 T1–T4). Sulfide ores exhibit crystalline, metasomatic, emulsion, graphic, heterogranular, and cataclastic textures, with massive, disseminated, brecciated, veined, and banded structures (Wang et al. 2000; Zhu et al. 2016). Ores of the Tianbaoshan deposit have undergone diagenetic, hydrothermal, and oxidized phases of development. The hydrothermal period involved sulfide–quartz, sulfide–carbonate, and carbonate stages. Two principal mineral assemblages, pyrite–chalcopyrite–arsenopyrite–quartz and sphalerite–galena–pyrite–calcite, formed in the sulfide–quartz and sulfide–carbonate stages, respectively (Wang et al. 2000; Zhou et al. 2013a). In the pyrite–chalcopyrite–arsenopyrite–quartz assemblage, pyrite is fine-grained (0.1–0.5 mm) with xenomorphic granular textures. In the sphalerite–galena–pyrite–calcite assemblage, sphalerite is fine- to coarse-grained (0.06–11 mm) with xenomorphic to automorphic granular textures, and is brown to yellow in color; galena has xenomorphic to automorphic granular textures (Wang et al. 2000; Zhou et al. 2013a). Wall-rock alteration includes dolomitization, calcitization, silicification, and ferritization, of which dolomitization, calcitization, and silicification are closely associated with Pb–Zn mineralization (ESM 1; Zhou et al. 2013a).

The Fusheng deposit

In the Fusheng ore field, the stratigraphic sequence includes Quaternary, Lower Triassic, and Permian strata (Fig. 2b). The Lower Permian Maokou Formation is the principal ore-hosting sequence and predominantly comprises gray dolomitic limestone and dolostone overlain by middle Permian Emeishan flood basalts. The Emeishan flood basalts are in turn overlain by the upper Permian Xuanwei Formation, which comprises mainly sandstone, siltstone, and shale. The Lower Triassic Feixianguan and Yongningzhen formation strata comprise siltstone, shale, dolostone, mudstone, and limestone. Two fault systems are present in this area with N–S- and NE–SW-trending faults, which all formed during post-ore stages (Fig. 2b).

The Fusheng orebodies are 50–200 m long, 20–80 m wide, and 0.2–7 m thick. They are stratabound and lenticular in shape, with local pinching and swelling. Ores in the Fusheng deposit are dominantly sulfide ores, with small

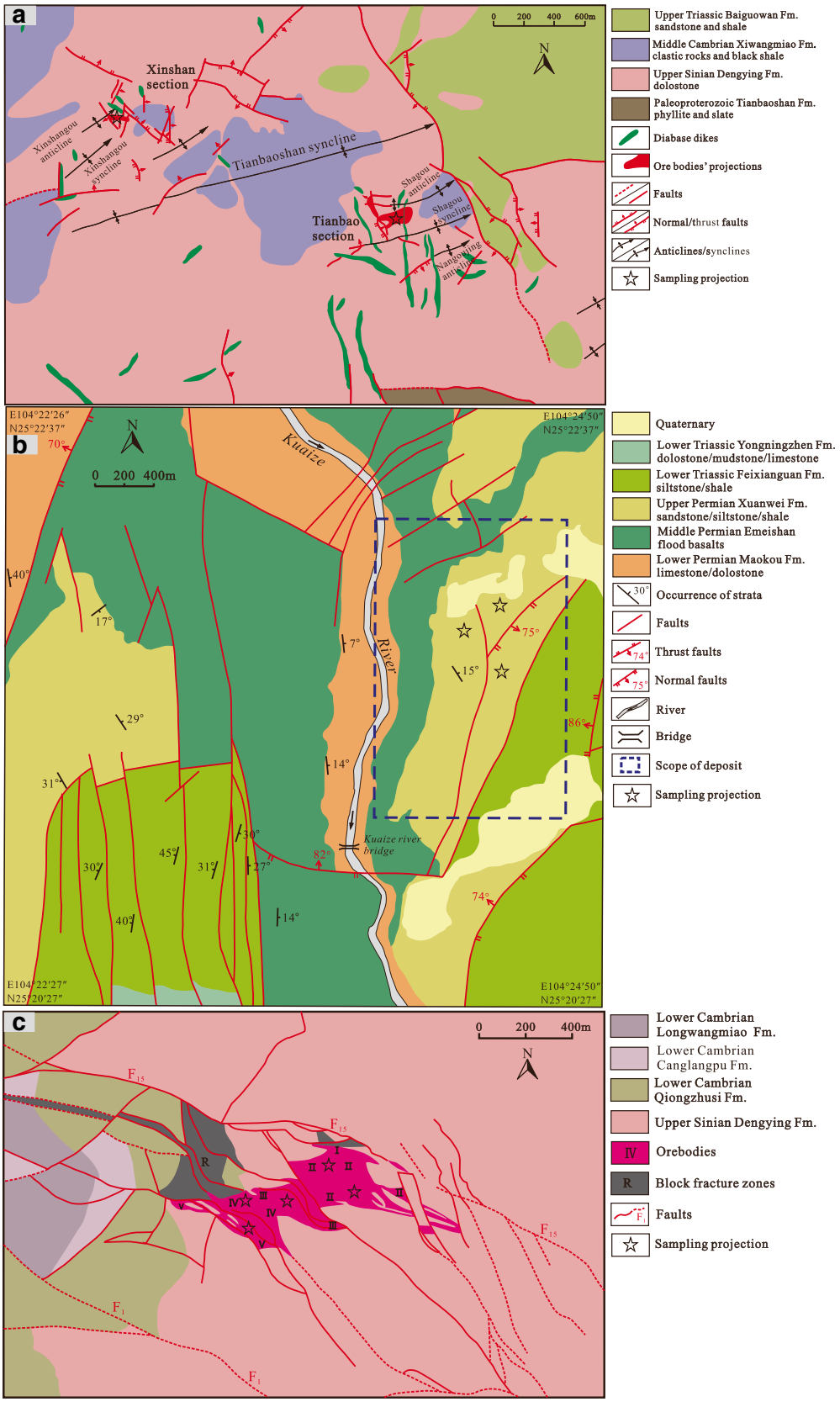

Fig. 2 (**a**) Geological map of the Tianbaoshan deposit (after He et al. 2016). (**b**) Geological map of the Fusheng deposit. (**c**) Geological map of the Daliangzi deposit (after Zhang et al. 2015)

amounts of oxidized ores near the faults. The ore mineralogy is relatively simple and includes mainly sphalerite, galena, pyrite, calcite, and dolomite (Fig. 4 F1–F4). Sulfide ores exhibit brecciated, massive, disseminated, and veined structures, of which brecciated ore is the dominant type (Fig. 4 F1, F2). The principal ore minerals have colloform, microcrystalline to coarsely crystalline granular, and euhedral–subhedral–anhedral granular textures (Fig. 4 F3, F4). The mineralization has been divided into three stages (Si 2005): a sedimentary diagenetic stage, including sedimentary pyrite in host carbonate rocks; a hydrothermal ore-forming stage, including sphalerite, galena, pyrite, dolomite, and calcite; and a supergene stage, including smithsonite and dolomite.

Sphalerite is fine-grained to macrocrystalline, euhedral to anhedral, with grain sizes of 0.1–10 mm. It occurs in brecciated, massive, banded, and disseminated aggregates together with galena, pyrite, dolomite, and calcite. Galena is fine-grained to macrocrystalline, euhedral to subhedral or subhedral to anhedral, with grain sizes of 1–30 mm (Fig. 4 F3). Dolomite occurs as coarse-grained crystals (1–3 mm) in euhedral–subhedral granular aggregates and occurs primarily in massive and banded aggregates and as veinlets within orebodies (Fig. 4 F1, F2, F3). Calcite occurs mainly in dolomite, and sometimes as veinlets within massive sphalerite and galena. Wall-rock alteration includes dolomitization, calcitization, and silicification.

The Daliangzi deposit

The stratigraphic sequence in the Daliangzi ore district includes Quaternary, Lower Cambrian, and upper Sinian strata (Fig. 2c). The upper Sinian Dengying Formation is the principal ore-hosting sequence. It is up to 473 m thick and contains thin-bedded to massive dolostone, thin-bedded muddy siltstone, P-bearing dolostone, phosphate rock, and quartz-banded dolostone. The overlying Lower Cambrian Qiongzhusi, Canglangpu, and Longwangmiao formations contain mainly sandstone, shale, and dolostone. The ore district is located in a graben with many fissures and fractures, with faults F_1 and F_{15} (branches of the Xiaojiang fault belt) being the largest (Fig. 2c). The area to the north of F_1 and south of F_{15} is a fault block structure containing another 40 faults, including some block fracture zones (R in Fig. 2c). The orebodies are closely related to the fractures and block fracture zones. No igneous rocks crop out in the mine area, although middle Permian Emeishan basalts occur on the northwest outer margin of the district.

The Daliangzi deposit contains five orebodies occurring as veins cross-cutting the bedding. The ore mineralogy is relatively simple and includes mainly sphalerite, galena, pyrite, calcite, and dolomite (Fig. 4 D1–D4). The major ore minerals are sphalerite and galena, associated with minor pyrite, chalcopyrite, arsenopyrite, marcasite, freibergite, and pyrargyrite. Gangue minerals are primarily dolomite and calcite, with minor quartz. The ores have massive, brecciated, and disseminated structures and occur as stockwork. Ore textures are fine-grained, spherulitic, framboidal, metasomatic, and emulsion. The ores generally occur as cavity or fracture fillings in dolomitic wall rocks. The mineralization has been divided into sedimentary, hydrothermal, and weathering periods (Zheng and Wang 1991). Minerals formed during the sedimentary period include dolomite, rare pyrite, and sphalerite. The hydrothermal period can be subdivided into three stages: pyrite–arsenopyrite, sphalerite–galena, and sphalerite–quartz. In the pyrite–arsenopyrite stage, a mineral association of pyrite + arsenopyrite + chalcopyrite + marcasite + quartz was formed. During the sphalerite–galena stage, an association of sphalerite + galena + chalcopyrite + calcite + quartz was formed (Zheng and Wang 1991). Minerals with a higher degree of idiomorphism, formed in the sphalerite–quartz stage, include sphalerite, calcite, quartz, and galena. The deposit was weathered after formation and formed a mineral association comprising mainly smithsonite and cerussite (Zheng and Wang 1991). Wall-rock alteration includes silicification, dolomitization, calcitization, and pyritization distributed locally in orebodies and wall rocks.

The Maozu deposit

Orebodies of the Maozu deposit are hosted in dolostone of the upper Sinian Dengying Formation and are structurally controlled by Maozu fold-and-thrust tectonic fractures (Fig. 3 D–1). In the Maozu ore field, upper Sinian carbonates and Cambrian sediments (dominantly sandstone, limestone, and black shale) formed the Ganshulin and Baika synclines, and Hongfadong and Changpo anticlines (Fig. 3 D–1). The Ganshulin, Baika, Hongfadong, and Changpo structures trend axially NNE or NE. Four orebodies are delineated in the upper part of the Dengying Formation and five in the lower part, with one body being 240–930 m long, 45–725 m wide, and 1.7–8.3 m thick and containing 0.77–6.11 wt% Pb and 3.85–11.48 wt% Zn. The orebodies are stratabound and located within wall-rock boundaries or occur as veins cross-cutting the bedding (Fig. 3 D–2; Liu 2009).

Ores are predominantly sulfides, with small amounts of oxidized ores, and their mineralogy includes sphalerite, galena, pyrite, and chalcopyrite, with calcite, dolomite, and quartz as gangue minerals (Fig. 4 M1–M4). Sulfide ores have euhedral–subhedral–anhedral granular, metasomatic, colloform, and mosaic textures; with massive, disseminated, banded, and veined structures. Mineralization can

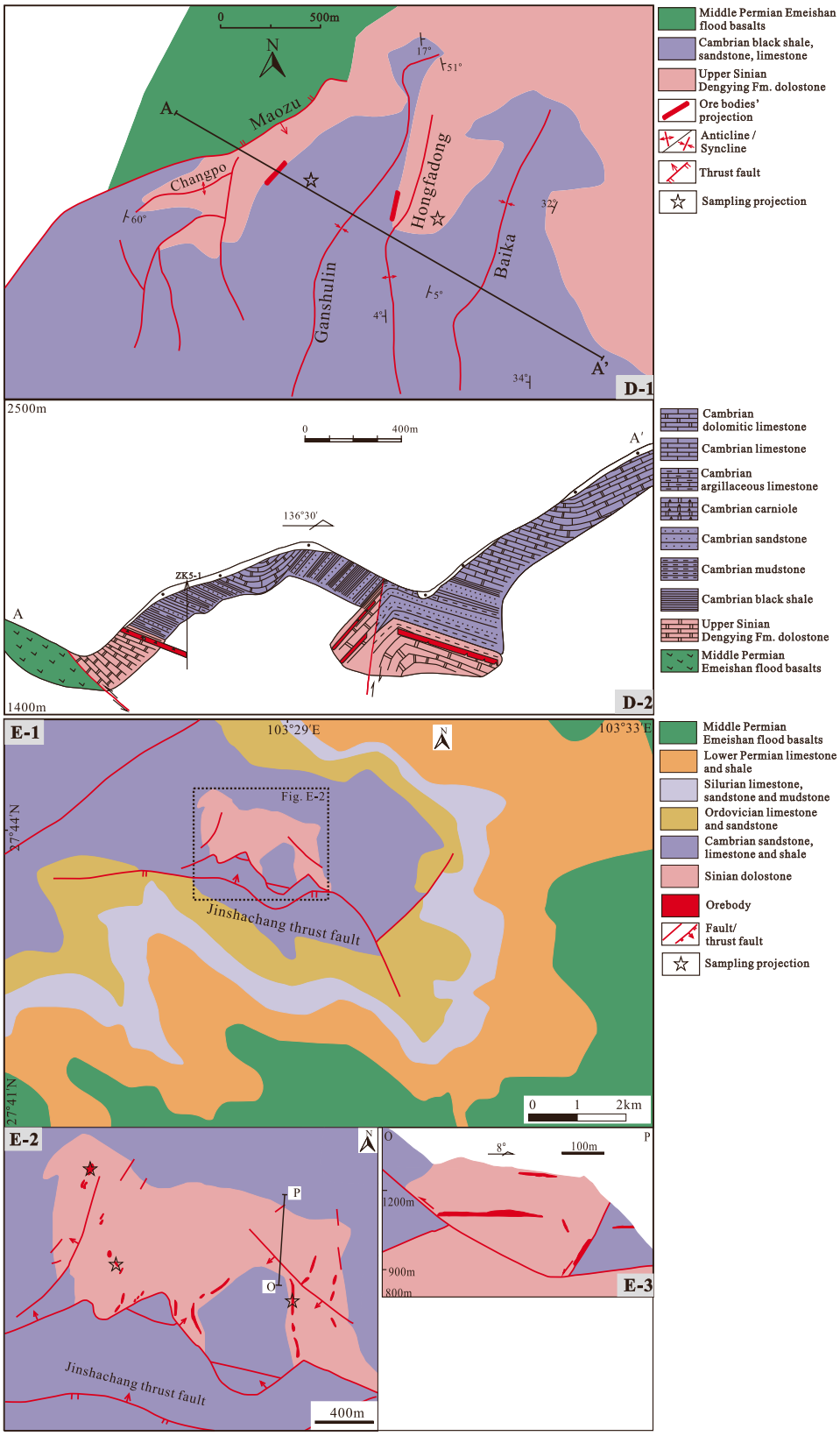

Fig. 3 (D-1) Geological map of the Maozu deposit (after Zhou et al. 2013d). (D-2) A-A′ cross section of the Maozu deposit (after Zhou et al. 2013d). (E-1) Geological map of the Jinshachang area (after Zhou et al. 2015). (E-2) Geological map of the Jinshachang deposit (after Zhou et al. 2015). (E-3) Cross section (O–P) of the Jinshachang deposit (after Zhang et al. 2015)

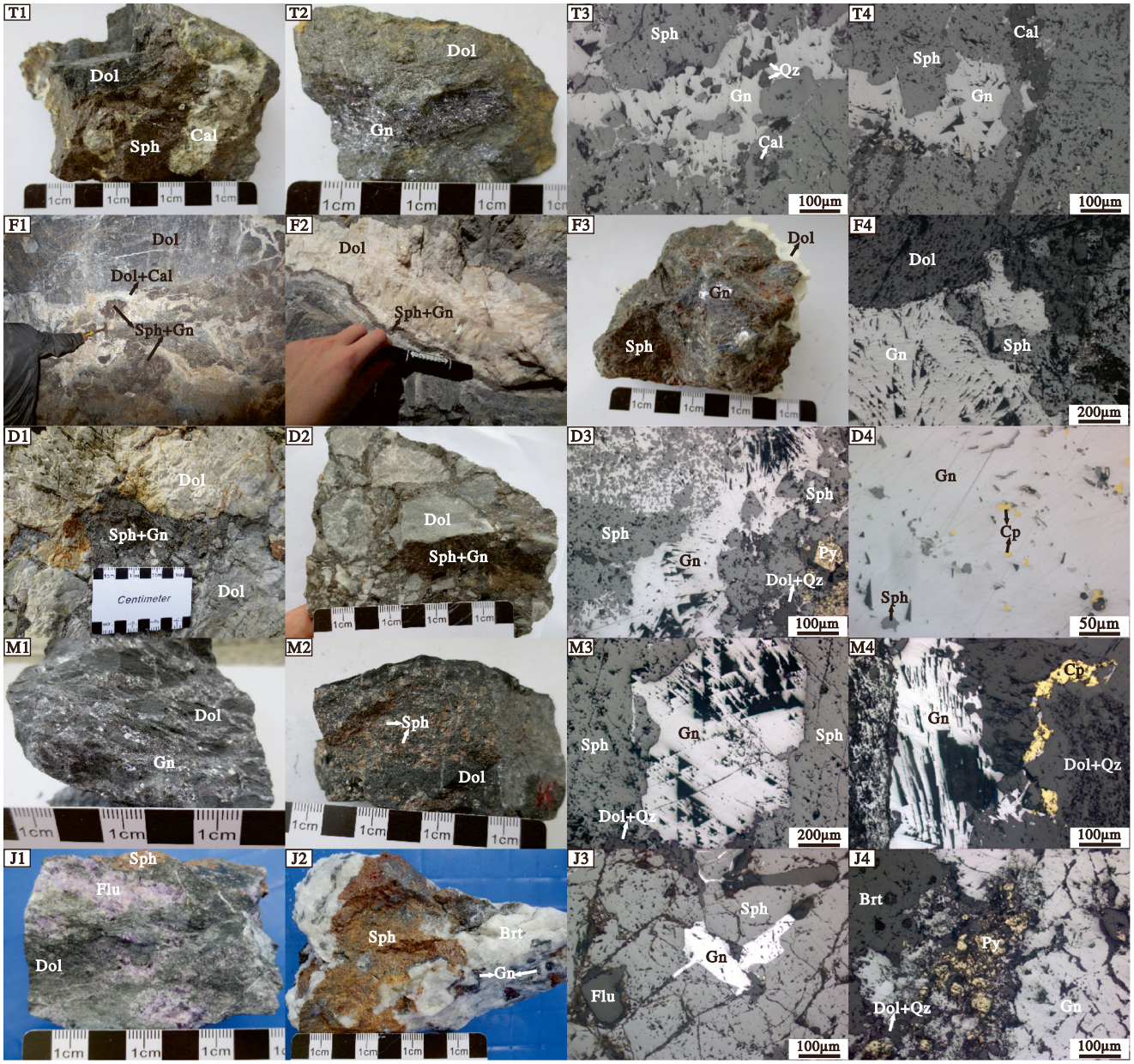

Fig. 4 Field, ore, and microscopic pictures of the Tianbaoshan (T1–T4), Fusheng (F1–F4), Daliangzi (D1–D4), Maozu (M1–M4) and Jinshachang (J1–J4) Pb-Zn deposits. (T1) breccia Zn-Pb ore; (T2) massive Zn-Pb ore; (T3) metasomatic sphalerite and galena–granular quartz–patch calcite; (T4) vein calcite in the early stage sphalerite and galena. (F1) field photograph of ore body; (F2) sphalerite and galena vein in dolomite; (F3) disseminated galena with patchy sphalerite and dolomite; (F4) metasomatic sphalerite and galena in patch dolomite. (D1) Oxidized ores in host rocks; (D2) breccia Zn–Pb ore; (D3) metasomatic sphalerite and galena–patch dolomite and quartz–granular pyrite; (D4) photomicrograph showing massive galena and spotted chalcopyrite and sphalerite. (M1) disseminated galena in dolostone; (M2) disseminated sphalerite in dolostone; (M3) metasomatic sphalerite and galena–patch dolomite and quartz; (M4) metasomatic sphalerite and patch chalcopyrite in dolomite and quartz. (J1) patchy fluorite and sphalerite in dolostone; (J2) disseminated galena and patchy sphalerite in barite; (J3) patchy fluorite in granular sphalerite and galena; (J4) metasomatic sphalerite and barite–xenomorphic granular pyrite. Mineral abbreviations: Brt, barite; Cal, calcite; Cp, chalcopyrite; Dol, dolomite; Flu, fluorite; Gn, galena; Py, pyrite; Qz, quartz; Sph, sphalerite

be considered in terms of diagenetic, hydrothermal, and oxidized periods, of which the hydrothermal period can be further subdivided into sulfide–carbonate–quartz and carbonate stages. For the sulfide–carbonate–quartz stage, mineral assemblages are pyrite–sphalerite–dolomite, quartz–sphalerite–chalcopyrite–galena–dolomite, and sphalerite–galena–dolomite–quartz (Fig. 4 M1–M4; Zhou et al. 2013d). Wall-rock alteration involved mainly

dolomitization, calcitization, Fe–Mn carbonatization, and ferritization, of which dolomitization and calcitization were closely associated with Pb–Zn mineralization, and Fe–Mn carbonatization and ferritization are the important indicators for ore prospecting at the surface (Zhou et al. 2013d).

The Jinshachang deposit

The stratigraphic sequence in the Jinshachang ore district includes Sinian dolostone; Cambrian sandstone, limestone, and shale; Ordovician limestone and sandstone; Silurian limestone, sandstone, and mudstone; lower Permian limestone and shale; and middle Permian Emeishan flood basalts. Mineralization is hosted by upper Sinian Dengying dolostones and lower Cambrian Meishucun phosphoric dolostones located in areas associated with the NW–SE-trending Jinshachang anticline, WNW–ESE-trending Jinshachang thrust fault, and several second-order faults around the deposit (Fig. 3 E–1, E–2).

The deposit contains ~ 0.42 Mt of Pb–Zn and comprises 27 orebodies. The main orebodies are 72–665 m long, 137–175 m wide, 1–6 m thick, and with grades of 0.79–10.76 wt% Zn, 1.56–7.14 wt% Pb, and 14.1–128.3 g t^{-1} Ag (Guo 2007). The orebodies dip at 5°–25°, and most form stratabound lenses within interlayered fracture zones. Several small vein-like orebodies are associated with second-order faults (Fig. 3 E–3).

Ores include sulfide and oxidized ores and a mixture of these (Bai et al. 2013; Zhang et al. 2015), and mineralization can be considered in terms of hydrothermal and oxidized periods. Ore minerals include sphalerite, galena, and pyrite, with barite, fluorite, quartz, dolostone, and calcite as gangue minerals (Fig. 4 J1–J4). Sulfide ores are dominated by massive, disseminated, brecciated, and veined structures. The minerals display idiomorphic–hypidiomorphic–xenomorphic granular, metasomatic dissolution, intersertal, and cataclastic textures (Fig. 4 J3, J4; Bai et al. 2013; Zhang et al. 2015). Oxidized and mixed ores display complex assemblages of smithsonite, limonite, cerusite, sulfide, quartz, fluorite, barite, and carbonate minerals (Bai et al. 2013; Zhang et al. 2015). The hydrothermal period can be divided into pyrite–silicified dolostone, sulfide–barite–fluorite, and barite–fluorite–quartz stages, with the second being the main stage containing sphalerite–fluorite (Fig. 4 J1), sphalerite–galena–barite (Fig. 4 J2), sphalerite–galena–fluorite (Fig. 4 J3), and galena–barite–fluorite (Fig. 4 J4; Bai et al. 2013; Zhou et al. 2015). Wall-rock alteration includes silicification, fluoritization, baritization, and dolomitization (Bai et al. 2013; Zhang et al. 2015).

Sampling and analytical methods

Sample collection and preparation

Representative samples from different locations and ore types were collected from underground ore bodies of the studied Pb–Zn deposits. The approximate sampling positions are projected on surface as shown in Figs. 2 and 3. A total of 45 sphalerite samples from the Tianbaoshan (3), Fusheng (8), Daliangzi (17), Maozu (6), and Jinshachang (11) Pb–Zn deposits were analyzed for S, Pb, Zn, and Cd isotopes. Twenty-four galena (Tianbaoshan 2, Fusheng 4, Daliangzi 10, Maozu 2 and Jinshachang 6) and 2 Jinshachang barite samples coexisting with sulfides were analyzed for S isotopes.

Minerals were handpicked under a binocular microscope, and then crushed and pulverized in an agate mortar. Sphalerite separates analyzed for Zn and Cd isotopes were pretreated by chemical separation and purification to avoid interferences and matrix effects. Chemical separation and purification procedures were conducted at the State Key Laboratory of Ore Deposit Geochemistry (SKLODG), Institute of Geochemistry, Chinese Academy of Sciences, Guiyang, China. During these steps, 2–5 mg sphalerite powder samples was weighted into Savillex screw top beakers and then digested using a mixture of ultrapure HCl (2 ml) + HNO_3 (1 ml). After complete dissolution, 1 ml 8 N HCl was added to the beaker and then heated to dryness at 70–80 °C. This process was repeated two times to ensure that all cations were converted to chloride species (Huang et al. 2016). The final residues were dissolved in 1 ml 8 N HCl and 3 ml 2 N HCl in preparation for chemical separation and purification of zinc and cadmium, respectively. Zinc and cadmium were extracted by pre-cleaned 100–200 mesh AG-MP-1M (3 ml, chloride form) anion exchange resin, using a procedure adapted from Maréchal et al. (1999) and Wen et al. (2016), respectively. After chemical separation and purification, the Zn and Cd fractions were dissolved in 2 ml 2% HNO_3 in preparation for isotope analysis. All reagents were purified in an ultra-clean laboratory; HNO_3 and HCl were purified by sub-boiling distillation; and Milli-Q H_2O (18.2 MΩ) was used.

Sulfur isotopic analysis

Sulfur isotope analyses were performed using an EA-MAT-253 mass spectrometer at the SKLODG. Samples were combusted with copper oxide under vacuum at 1000 °C to produce SO_2 which was used for the gas mass spectrometer measurements (Robinson and Kusakabe 1975). S isotopic compositions are reported relative to the Vienna Canyon Diablo Troilite (V–CDT) international

standard. Sulfur isotopic data are reported in standard δ–notation in per mil: $\delta^{34/32}S = [(^{34}S/^{32}S)_{sample}/(^{34}S/^{32}S)_{V\text{-}CDT} - 1] \times 1000‰$. Measured $\delta^{34}S$ ($\delta^{34}S = \delta^{34}S_{VCDT} = \delta^{34/32}S$) values of IAEA-S1, IAEA-S2, and IAEA-S3 standards are $-0.09‰ \pm 0.16‰$, $22.49‰ \pm 0.21‰$, and $-32.59‰ \pm 0.16‰$ (mean ± 2SD; 2SD stands for two times the standard deviation of the population of duplicate measurements of a sample solution), respectively. These values agree well with those reported previously (Zhu et al. 2016).

Lead isotopic analysis

Lead isotopic measurements were conducted on a Neptune Plus multi-collector inductively coupled plasma mass spectrometer (MC–ICP–MS) at the SKLODG. For Pb isotopic analysis, sphalerite separates were crushed and pulverized in an agate mortar, followed by decomposition using a mixture of ultrapure HNO_3 and HCl. After incipient dryness, decomposed samples were dissolved in HCl for Pb column separation using conventional ion exchange chromatography (Zhu et al. 2018). Samples were doped with Tl to facilitate corrections for instrumental mass bias based on an exponential mass law dependence. Duplicate analyses of the NBS-981 Pb isotopic standard gave a reproducibility of $^{206}Pb/^{204}Pb = 16.9360 \pm 0.0063$, $^{207}Pb/^{204}Pb = 15.4898 \pm 0.0086$, and $^{208}Pb/^{204}Pb = 36.7029 \pm 0.0263$ (mean ± 2SD), in agreement with reference values reported previously (Belshaw et al. 1998; Zhou et al. 2013a, 2013b, 2013d, 2013e; Gao et al. 2018).

Zinc isotopic analysis

Zinc isotopic analyses were carried out using a Neptune Plus MC–ICP–MS at the SKLODG. The sample standard bracketing method was used for Zn isotopic analyses to correct for instrumental mass fractionation (Zhu et al. 2002; Schoenberg and Von 2005; Borrok et al. 2007; Li et al. 2008; Dauphas et al. 2009; Duan et al. 2016). Zn concentrations in samples and reference standards (IRMM-3702) were matched to within 10%. Analyses were conducted in static mode; blank signals were subtracted from each of the measured masses; instrumental drift was corrected by averaging ratios measured in bracketing reference solutions; and only sections with linear or smooth drifts for the reference solution were used to calculate sample δ values. IRMM-3702 was used as an internal reference standard and CAGS Zn as a secondary reference material. Zinc isotopic data are reported in standard δ–notation in per mil: $\delta^{x/64}Zn = [(^{x}Zn/^{64}Zn)_{sample}/(^{x}Zn/^{64}Zn)_{IRMM\text{-}3702} - 1] \times 1000‰$, where ^{x}Zn means the ^{66}Zn, ^{67}Zn, or ^{68}Zn isotope. Repeated measurements of the CAGS Zn solution gave a $\delta^{66/64}Zn$ ($\delta^{66}Zn$) value of $-0.87‰ \pm 0.08‰$ (mean ± 2SD), within the range of previous determinations (−0.77 to −0.87‰; Tang et al. 2016). The $\delta^{68}Zn$–$\delta^{66}Zn$ diagram (Fig. 5a) shows that Zn isotopic compositions of all sphalerite samples plot within error limits of the theoretical equilibrium mass fractionation lines, indicating that isobaric interference was effectively removed by chemical purification and correction during analysis. All $\delta^{66}Zn$ values are reported relative to the JMC Lyon Zn standard 3-0749 L ($\delta^{66}Zn_{JMC\text{-}Lyon} = \delta^{66}Zn_{IRMM\text{-}3702} + 0.32$; ESM 2).

Cadmium isotope analysis

Cadmium isotopic analyses were performed on a MC–ICP–MS at the SKLODG. Matrix effects, concentration effects, and medium effects during Cd isotopic analysis have been studied previously by Wombacher et al. (2003, 2004) and Christophe et al. (2005). Here, the standard sample bracketing method was again used, with concentrations in samples and standards (NIST SRM-3108 Cd) being matched to within 10%. This and other conditions were the same as those reported for Zn in the "Zinc isotopic analysis" section. NIST SRM 3108 Cd was used as an

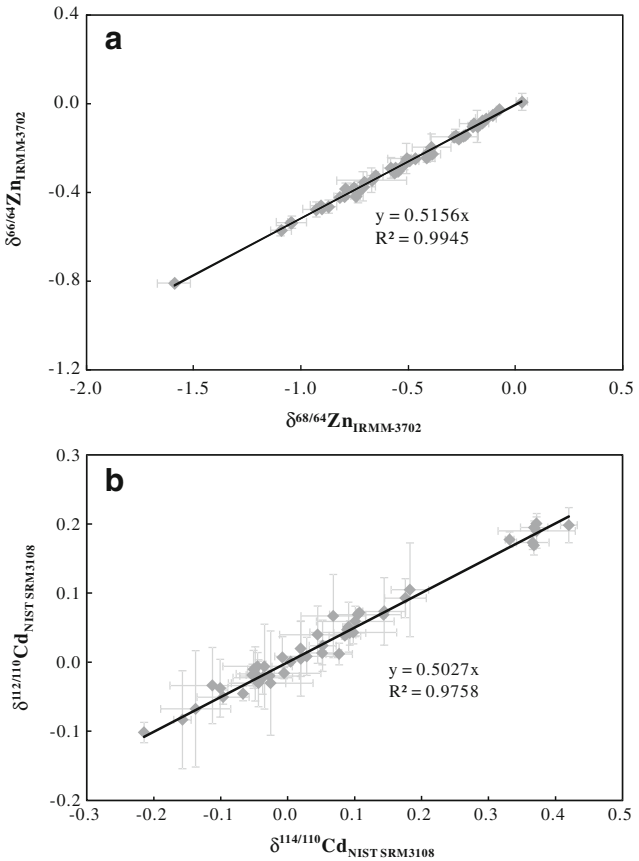

Fig. 5 **a** Diagrams of $\delta^{68/64}Zn$ vs $\delta^{66/64}Zn$ of the sphalerite samples from the studied deposits, and all samples are within the error of the theoretical mass fractionation line (TMFL). **b** Diagrams of $\delta^{114/110}Cd$ vs $\delta^{112/110}Cd$ of the sphalerite samples from the studied deposits, and all samples are within the error of the theoretical mass fractionation line (TMFL)

internal reference standard, and JMC Cd as a secondary reference material. Standard δ notation, as defined by the relationship shown below, was used to present the results: $\delta^{x/110}Cd = [(^{x}Cd/^{110}Cd)_{sample}/(^{x}Cd/^{110}Cd)_{NIST\ SRM\ 3108} - 1] \times 1000‰$, where ^{x}Cd means the ^{111}Cd, ^{112}Cd, ^{113}Cd, or ^{114}Cd isotope. Repeated measurements of the JMC Cd solution gave a $\delta^{114/110}Cd$ ($\delta^{114}Cd$) value of − 1.63‰ ± 0.05‰ (mean ± 2SD), within the previously reported range of − 1.56 to − 1.63‰ for this solution (Abouchami et al. 2012; Zhang et al. 2016). The $\delta^{114}Cd$–$\delta^{112}Cd$ diagram (Fig. 5b) shows that the Cd isotopic compositions of all sphalerite samples fall within error limits of the theoretical equilibrium mass fractionation lines, indicating that isobaric interferences were effectively removed by chemical purification and correction during analysis. All $\delta^{114}Cd$ values are reported relative to the Spex Cd standard ($\delta^{114}Cd_{Spex} = \delta^{114}Cd_{NIST\ SRM\ 3108} + 0.11$; ESM 2).

Results

Sulfur isotopic composition

Sphalerite separates from the Tianbaoshan, Fusheng, Daliangzi, Maozu, and Jinshachang Pb–Zn deposits have $\delta^{34}S$ values (*n*, mean ± 1σ; *n* is the number of samples, 1σ is the standard deviation of values for n sample) of + 4.3 to + 5.4‰ (*n* = 3, + 4.8‰ ± 0.6‰), + 14.5 to +15.9‰ (*n* = 8, + 15.1‰ ± 0.4‰), + 14.3 to + 15.8‰ (*n* = 17, + 14.9‰ ± 0.4‰), + 12.4 to + 14.0‰ (*n* = 6, + 12.9‰ ± 0.6‰), and + 4.0 to + 12.6‰ (*n* = 11, + 7.1‰ ± 2.9‰) (ESM 2), while galena has $\delta^{34}S$ values of + 2.2 to +3.2‰ (*n* = 2, + 2.7‰ ± 0.7‰), + 9.2 to + 11.5‰ (*n* = 4, + 10.9‰ ± 1.1‰), + 10.8 to + 12.2‰ (*n* = 10, + 11.4‰ ± 0.5‰), + 5.9 to + 11.7‰ (*n* = 2, + 8.8‰ ± 4.1‰), and + 3.0 to + 7.2‰ (*n* = 6, + 4.7‰ ± 1.6‰) (ESM 3), respectively. Barite separates from the Jinshachang deposit have $\delta^{34}S$ values of + 20.8 to + 32.6‰ (*n* = 2, + 26.7‰ ± 8.4‰) (ESM 3; Fig. 6).

Pb isotopic composition

Sphalerite separates from the Tianbaoshan, Fusheng, Daliangzi, Maozu, and Jinshachang deposits have $^{206}Pb/^{204}Pb$, $^{207}Pb/^{204}Pb$, and $^{208}Pb/^{204}Pb$ ratios, respectively, as follows (ESM 2): 18.4155–18.4371, 15.7244–15.7272, and 38.761–38.771; 18.5637–18.6078, 15.6887–15.6939, and 38.563–38.586; 18.2364–20.2592, 15.6810–15.8405, and 38.478–40.466; 18.2112–19.6482, 15.6762–15.7859, and 38.407–39.824; and 20.6093–21.1834, 15.8516–15.8976, and 40.768–41.442. Pb isotopic compositions of sphalerite separates from the Jinshachang deposit are much more radiogenic than those from the other deposits (Fig. 7).

Zn isotopic composition

Sphalerite separates from the Tianbaoshan, Fusheng, Daliangzi, Maozu, and Jinshachang deposits have $\delta^{66}Zn$ values (*n*, mean ± 1σ) of + 0.23 to + 0.26‰ (*n* = 3, + 0.24‰ ± 0.01‰), + 0.09 to + 0.33‰ (*n* = 8, + 0.23‰ ± 0.08‰), − 0.21 to + 0.22‰ (*n* = 17, − 0.01‰ ± 0.13‰), − 0.49 to − 0.10‰ (*n* = 6, − 0.22‰ ± 0.15‰), and − 0.05 to + 0.16‰ (*n* = 11, + 0.05‰ ± 0.06‰), respectively (ESM 2). $\delta^{66}Zn$ values of upper Sinian to lower Permian sedimentary whole-rock samples range from − 0.24 to + 0.32‰, with a mean of + 0.11‰ ± 0.18‰ (Zhou et al. 2014b; He et al. 2016; He 2017). In contrast, Sedimentary whole-rock samples from the Proterozoic folded basement and Permian Emeishan flood basalts samples have whole-rock $\delta^{66}Zn$ values of + 0.07 to + 0.62‰, + 0.32 to +0.44‰, with a mean of + 0.35‰ ± 0.08‰, + 0.29‰ ± 0.18‰, respectively (Zhou et al. 2014b; He 2017).

Cd isotopic composition

Sphalerite separates have an overall range in $\delta^{114}Cd$ values of − 0.10 to +0.53‰, with a variation of 0.63‰ and mean of + 0.18‰ ± 0.16‰ (ESM 2). Sphalerite from the Tianbaoshan, Fusheng, Daliangzi, Maozu, and Jinshachang deposits has $\delta^{114}Cd$ values (*n*, mean ± 1σ) of + 0.25 to + 0.29‰ (*n* = 3, + 0.28‰ ± 0.02‰), + 0.07 to + 0.53‰ (*n* = 8, + 0.40‰ ± 0.17‰), − 0.10 to + 0.44‰ (*n* = 17, + 0.11‰ ± 0.13‰), − 0.05 to +0.10‰ (*n* = 6, + 0.05‰ ± 0.06‰), and + 0.08 to + 0.22‰ (*n* = 11, + 0.16‰ ± 0.05‰), respectively (ESM 2).

Discussion

Possible sources of sulfur

Primary ores in the Tianbaoshan, Fusheng, and Daliangzi Pb–Zn deposits have a simple S mineralogy that lacks sulfates. $\delta^{34}S\Sigma_{S-fluid}$ values of the Tianbaoshan, Fusheng, and Daliangzi deposits, calculated from $\delta^{34}S$ values of sphalerite and coexisting galena, are + 4.2‰ (Zhu et al. 2016), + 14.6‰, and + 10.3‰, respectively. Besides, in the temperature range 110–290 °C, the $\delta^{34}S$ value of sphalerite is very similar to that of original ore-forming fluid (Ohmoto and Rye 1979; Seal 2006), so the average $\delta^{34}S$ value of sphalerite may alternatively be used as an estimate of the fluid value. The $\delta^{34}S$ values of ore-forming fluid determined by these two methods are very similar. The largest difference occurs in the Daliangzi deposit, where the average $\delta^{34}S$ value of sphalerite is only 4.6‰ greater than the fluid value calculated from sphalerite and coexisting galena. This observation indicates that sulfur isotopic compositions of sulfides could reflect

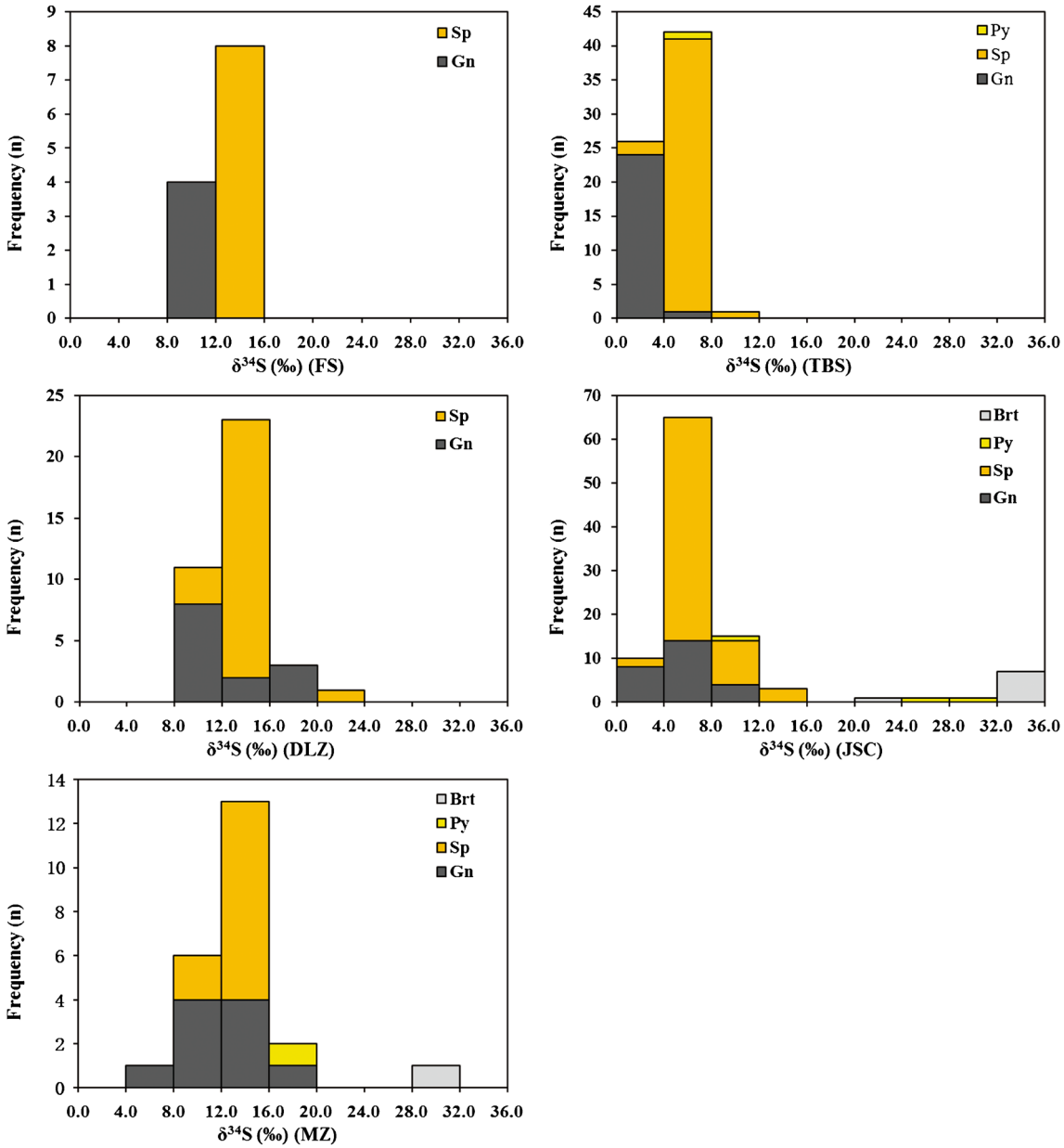

Fig. 6 Histogram of $\delta^{34}S$ values of sulfur-bearing minerals from the Tianbaoshan (TBS), Fusheng (FS), Daliangzi (DLZ), Maozu (MZ), Jinshachang (JSC) Pb-Zn deposits. The sources of published data are as follows: Daliangzi (Yuan et al. 2014), Jinshachang (Tu 1984; Liu and Lin 1999; Bai et al. 2013), Maozu (Liu and Lin 1999; Liu 2009; Zhou et al. 2013d), Tianbaoshan (Fu 2004; Zhou et al. 2013a; Zhu et al. 2016)

ore-forming fluid ($\delta^{34}S\Sigma_{S-fluid}$) values (Ohmoto 1972) of the Tianbaoshan, Fusheng, and Daliangzi Pb–Zn deposits.

Assuming sulfide precipitation under thermal equilibrium conditions, isotopic fractionation factor (α) given by Ohmoto and Rye (1979) may be used to calculate the temperature of formation of the coexisting sphalerite–galena pairs:

$$1000\ln\alpha_{Sp-Gn} = 0.73 \times 10^6/T^2,$$

where $1000\ln\alpha_{Sp-Gn} \approx \Delta^{34}S_{Sp-Gn}$ and $T = {}^{\circ}K$

Calculated ore-forming temperatures for the Tianbaoshan, Fusheng, and Daliangzi deposits are 121–288 °C (average 191 °C), 151–196 °C (171 °C), and 128–182 °C (163 °C) (ESM 4; Clayton 1981), respectively. These temperatures are roughly consistent with homogenization temperatures based on previous fluid inclusion studies of the Tianbaoshan (80–275 °C; Yu 2014), Fusheng (130–240 °C; Si 2005), and Daliangzi (140–230 °C; Zheng and Wang 1991) deposits (ESM 1), indicating that precipitation of sulfide minerals occurred under conditions of S isotopic equilibrium.

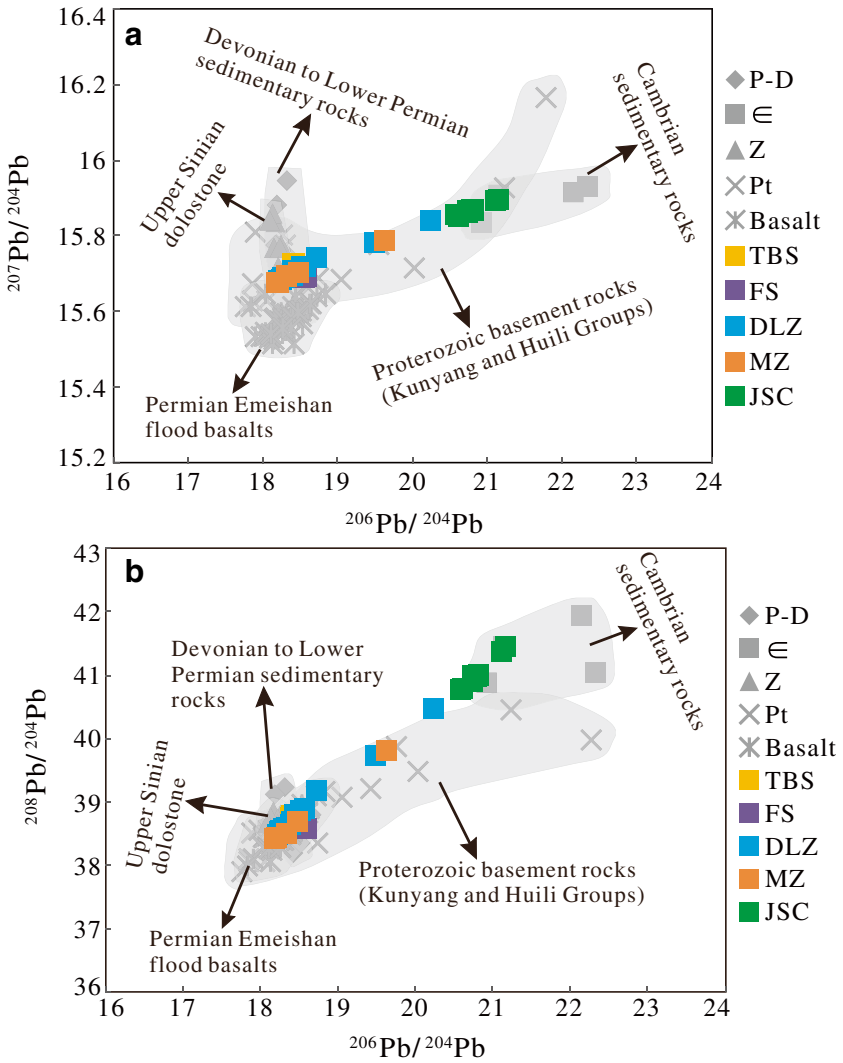

Fig. 7 **a** Plots of $^{207}Pb/^{204}Pb$ vs $^{206}Pb/^{204}Pb$ of sphalerite samples from the studied Pb-Zn deposits. **b** Plots of $^{208}Pb/^{204}Pb$ vs $^{206}Pb/^{204}Pb$ of sphalerite samples from the studied Pb-Zn deposits. Data of the bulk-rock Pb isotopic compositions are from Zheng and Wang (1991), Zhang et al. (1998), Hu (1999), Liu and Lin (1999), Fu (2004), Huang et al. (2004), Han et al. (2007a), Yan et al. (2007), Zhou et al. (2001, 2013d, 2013e), Huang et al. (2015), and Zhou et al. (2015). Lead isotopic ratios for sedimentary rocks and Emeishan flood basalts are age-corrected at 206 Ma. $(^{206}Pb/^{204}Pb)_t = (^{206}Pb/^{204}Pb)_p - \mu(e^{\lambda t}-1)$, $(^{207}Pb/^{204}Pb)_t = (^{207}Pb/^{204}Pb)_p - \mu/137.88(e^{\lambda' t}-1)$, $(^{208}Pb/^{204}Pb)_t = (^{208}Pb/^{204}Pb)_p - \omega(e^{\lambda'' t}-1)$, $\lambda = 1.55125 \times 10^{-10}\ t^{-1}$, $\lambda' = 9.8485 \times 10^{-10}\ t^{-1}$, $\lambda'' = 0.49475 \times 10^{-10}\ t^{-1}$, $t = 206$ Ma

Previous studies have obtained sulfide $\delta^{34}S$ values for the Tianbaoshan, Fusheng, Daliangzi, and Maozu Pb–Zn deposits of + 0.0 to + 9.6‰ (Fu 2004; Zhou et al. 2013a; Zhu et al. 2016), + 9.2 to + 15.9‰, + 9.7 to +20.6‰ (Yuan et al. 2014), and + 5.9 to +19.2‰ (Liu and Lin 1999; Liu 2009; Zhou et al. 2013d), respectively (Fig. 6; ESM 2 and 3). The Jinshachang deposit differs from the other four in that it contains sulfates (barite) coexisting with sulfides. Sulfide $\delta^{34}S$ values there (ESM 2 and 3) are + 1.1 to + 13.4‰ (Tu 1984; Liu and Lin 1999; Bai et al. 2013), while barite $\delta^{34}S$ values are + 20.8 to +35.2‰ (Bai et al. 2013), similar to those of Cambrian–Triassic seawater sulfates (+ 15 to + 35‰) and evaporates (+ 15 to + 30‰) in Cambrian–Triassic sedimentary strata (Claypool et al. 1980; Liu and Lin 1999; Seal 2006; Han et al. 2007a; Bai et al. 2013; Zhou et al. 2013d; Zhou et al. 2015).

The obviously lighter $\delta^{34}S$ values for the Tianbaoshan deposit indicate a different S source for this deposit. There are three interpretations concerning the source of S for the Tianbaoshan deposit: (1) a mixture of mantle and sedimentary rock sources (Guan and Li 1999; Kou et al. 2015); (2) TSR reaction of evaporates in host strata resulting in lower $\delta^{34}S$ values than the other SYG Pb–Zn deposits (Shao and Li 1997; Li 2003; Fu 2004; Zhang 2008; Wu 2013; Zhou et al. 2013a); and (3) reduced S leaching from the basement (Zhu et al. 2016). It has been confirmed that large amounts of volcanic or intrusive rocks (Meso–Neoproterozoic folded basement) exist beneath the Sinian Dengying Formation (Liu and Lin 1999; Fu 2004). Zheng and Wang (1991) suggested that S of the Daliangzi deposit is derived from Sinian seawater sulfate ($\delta^{34}S$ ~ + 20‰), where sulfate solution flowing through carbonate rock layers was reduced by organic matter to produce H_2S. Previous studies (Zhou et al. 2013d; Zhou et al. 2015) indicated that reduced S in hydrothermal fluids of the Maozu and Jinshachang deposits is derived predominantly from evaporates (gypsum and

barite) in Cambrian sedimentary strata (Liu and Lin 1999; Han et al. 2007b). The $\Delta^{34}S_{sulfate-sulfide}$ in sulfate reduction processes can be as high as + 10 to + 15‰ (Ohmoto et al. 1990; Ohmoto and Goldhaber 1997; Basuki et al. 2008).

In conclusion, it appears that S in the Tianbaoshan deposit originates mainly from the Meso–Neoproterozoic folded basement beneath the Dengying Formation; S in the Fusheng, Daliangzi, and Maozu deposits is derived mainly from evaporates or seawater sulfates in Cambrian–Triassic sedimentary strata; and S in the Jinshachang deposit may be derived from both folded basement and sulfates coexisting with sulfides. The distinct $\delta^{34}S$ values in the studied deposits are thus due to variable $\delta^{34}S$ values of evaporates in different host strata or to different ore-forming temperatures during TSR.

Possible sources of lead

U and Th contents of sulfide minerals are too low to influence their initial Pb isotopic compositions, whereas Pb isotopic compositions of the Proterozoic folded basement rocks, Cambrian, Devonian to Lower Permian sedimentary rocks and Middle Permian Emeishan flood basalts need to be corrected for ages. Geochronological studies on the SYG province show that the ages of Pb–Zn mineralization range between 226 and 166 Ma (Zhou et al. 2015; Zhou et al. 2013d, e) while the eruption age of the Emeishan basalts is ~ 260 Ma (Zhou et al. 2002; Zhong and Zhu 2006; Zhong et al., 2011). The initial Pb isotopic compositions for all the studied rocks are calculated to an age of 206 Ma, consistent with the treatment of Zhou et al. (2015).

In $^{207}Pb/^{204}Pb$–$^{206}Pb/^{204}Pb$ and $^{208}Pb/^{204}Pb$–$^{206}Pb/^{204}Pb$ diagrams (Fig. 7a, b), sphalerite data for the five deposits display linear correlations and overlap the upper Sinian dolostone and Devonian to lower Permian sediment fields. Data for most sphalerites of the Tianbaoshan, Fusheng, Daliangzi, and Maozu deposits plot in the upper Sinian dolostone and Devonian to lower Permian sediment fields. In contrast, several exceptional sphalerites from the Daliangzi and Maozu deposits plot in the Proterozoic basement field, while those from the Jinshachang deposit plot in the Proterozoic basement and Cambrian sediment fields (Fig. 7a, b). Most sphalerites of the Tianbaoshan, Fusheng, Daliangzi, and Maozu deposits overlap the field of Permian Emeishan flood basalts in the $^{208}Pb/^{204}Pb$–$^{206}Pb/^{204}Pb$ diagram (Fig. 7b), but not in the $^{207}Pb/^{204}Pb$–$^{206}Pb/^{204}Pb$ diagram (Fig. 7a). This suggests that Pb of the Tianbaoshan and Fusheng deposits originates predominantly from upper Sinian and Devonian to lower Permian sedimentary rocks; Pb of the Daliangzi and Maozu deposits has multiple sources including Proterozoic basement and upper Sinian and Devonian to lower Permian sedimentary rocks; and the more radiogenic Pb isotopic compositions of sphalerites from the Jinshachang deposit indicate that Pb there is most likely derived from Cambrian sedimentary rocks and Proterozoic basement. The Emeishan flood basalts are unlikely to have provided Pb for the studied deposits as they exhibit different ranges of Pb isotopic compositions. Moreover, large-scale hydrothermal alteration of the Emeishan basalts associated with the formation of these Pb-Zn deposits has not been reported yet.

Possible sources of zinc

Previous studies have indicated that Zn and Cd isotopes in sphalerite have similar isotopic fractionation mechanisms because of their similar chemical and crystallographic properties (Schwartz 2000; Yang et al. 2015; Zhu et al. 2015; Wen et al. 2016). Although cadmium concentration in the Earth's crust is extremely low (0.2 ppm; Tu et al. 2004), it can substitute extensively for Zn in sphalerite and is typically hosted in Pb-Zn deposits with concentrations of several hundred to several thousand ppm (Zhu et al. 2013). Therefore, Cd and Zn isotopes of the studied Pb-Zn deposits could be combined to demonstrate their possible sources of Zn. Three causes have been proposed to explain the variations of Zn and Cd isotope compositions in hydrothermal systems: (1) the sources (Wilkinson et al. 2005; Zhou et al. 2014a, b); (2) temperature effects (Mason et al. 2005; John et al. 2008; Toutain et al. 2008; Yang et al. 2015); and (3) isotopic fractionation during fluid evolution and mineral precipitation (Mason et al. 2005; Kelley et al. 2009; Gagnevin et al. 2012; Gao et al. 2018). The application of Zn and Cd isotopes in elucidating the formation of the SYG Pb–Zn deposits is discussed here, taking these considerations into account.

As aforementioned, the Daliangzi and Maozu deposits have the same Pb source, and their ore-forming fluid temperatures (140–230 °C and 153–248 °C, respectively), estimated in fluid inclusion studies (ESM 1), are generally similar. Furthermore, the almost linear correlation between sphalerite $^{206}Pb/^{204}Pb$ ratios and $\delta^{66}Zn$ values in the five deposits also indicates that Pb and Zn might originate from the same source rocks. However, $\delta^{66}Zn$ and $\delta^{114}Cd$ values of the Daliangzi (− 0.21 to + 0.22‰ and − 0.10 to + 0.44‰, respectively) and Maozu (− 0.49 to − 0.10‰ and − 0.05 to + 0.10‰, respectively) deposits are significantly different, suggesting that the $\delta^{66}Zn$ and $\delta^{114}Cd$ variations are most likely due to isotopic fractionation during fluid evolution and mineral precipitation, with precipitation temperature not exerting significant control of sphalerite Zn and Cd

isotopic compositions. This is consistent with the conclusions of Wilkinson et al. (2005) for the Irish ore field. In addition, Zn isotopic compositions of sedimentary rocks from Sinian to lower Permian strata exhibit similar ranges (− 0.24 to + 0.32‰; Fig. 8). It is therefore inferred that compositional variations in primary source rocks are not the main cause of variations in sphalerite Zn isotopic compositions.

In contrast, the Tianbaoshan deposit exhibits much heavier δ^{66}Zn values (+ 0.18 to + 0.73‰) than the other deposits (Fig. 8). A previous study presented that sedimentary rocks of the Proterozoic folded basement have δ^{66}Zn value of + 0.07 to + 0.62‰ (He et al. 2017; Fig. 8). The leaching experiments of Fernandez and Borrok (2009) demonstrated that the leached fluid is enriched in heavy Zn isotopes relative to the sphalerite-rich rocks (0.0 to + 0.2‰, $\Delta^{66}Zn_{solution\text{-}rock}$). Therefore, there are three explanations for the Zn isotopic characteristics of the Tianbaoshan deposit (Fig. 8): (1) Zn originates from Proterozoic folded basement; (2) Zn is derived from Sinian to lower Permian sedimentary rocks; (3) Zn has multiple sources, i.e., Sinian to lower Permian sedimentary rocks and Proterozoic folded basement, consistent with the conclusion of He (2016). In our opinion, the first explanation is unlikely as the above Pb isotopic compositions indicate that the metals are mainly derived from upper Sinian to lower Permian sedimentary rocks for this deposit. Alternatively, the second and third explanations are both possible because heavier δ^{66}Zn values could result from a later stage of fluid evolution and mineral precipitation in a hydrothermal fluid system. However, if the third explanation is reasonable only small amounts of Zn can be derived from Proterozoic folded basement as the lack of radioactive Pb in the Tianbaoshan Pb-Zn deposit.

Sphalerite Zn isotopic compositions in the Fusheng, Daliangzi, Maozu, and Jinshachang deposits range from − 0.25 to +0.33‰, overlapping the ranges of Sinian to lower

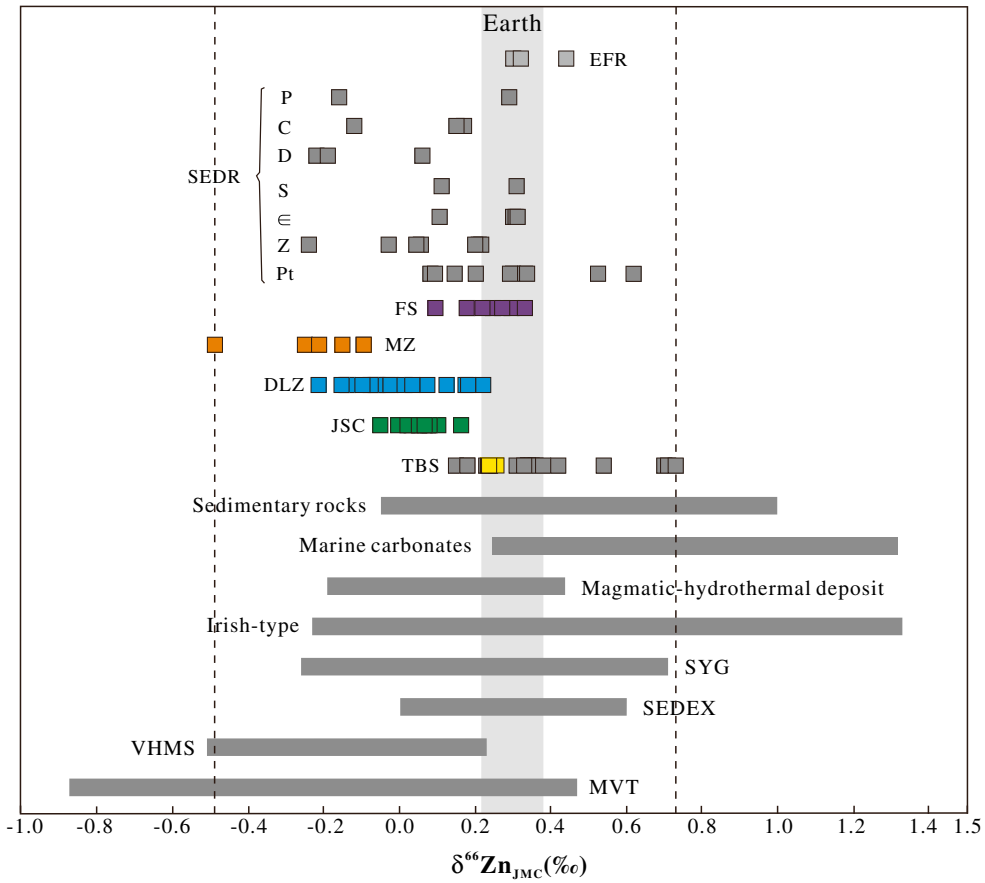

Fig. 8 Comparison of zinc isotopic compositions (δ^{66}Zn relative to JMC-Lyon) of sphalerite from the studied Pb-Zn deposits with data from various types of Pb-Zn deposits worldwide (after Duan et al. 2016; He et al. 2016). Data sources: TBS (He et al. 2016), sedimentary rocks (Maréchal et al. 2000; Weiss et al. 2007; Bentahila et al. 2008; Little et al. 2016; Lv et al. 2016), the Earth (Chen et al. 2013), Marine carbonate (Pichat et al. 2003), Irish-type (Wilkinson et al. 2005; Gagnevin et al. 2012), SEDEX (Kelley et al. 2009), magmatic-hydrothermal type (Maréchal et al. 1999; Duan et al. 2016; Li et al. 2017), VHMS (Jiang et al. 2001; Mason et al. 2005), MVT (Albarède 2004; Pašava et al. 2014), SYG (Zhou et al. 2014a, b; Zhou et al. 2016), EFR, SEDR (Zhou et al. 2014b; He 2017). Abbreviations: EFB, Permian Emeishan flood basalts; SEDR, Sedimentary rocks in the studied area; Pt, Proterozoic folded basement; Z, Sinian; ∈, Cambrian; S, Silurian; D, Devonian; C, Carboniferous; P, Permian; TBS, FS, DLZ, MZ, JSC are abbreviations of the Tianbaoshan, Fusheng, Daliangzi, Maozu, Jinshachang Pb-Zn deposits, respectively

Permian sedimentary rocks (except for one sample from the Maozu Pb–Zn deposit; − 0.49‰), but most samples have lighter Zn isotopic compositions than Emeishan flood basalts and Proterozoic folded basement (Fig. 8). In contrast, Fusheng sphalerites have heavier δ^{66}Zn values (+ 0.09 to +0.33‰) than Daliangzi, Maozu, and Jinshachang deposits (− 0.25 to + 0.22‰). As this deposit is hosted in lower Permian strata, its characteristics could correspond to a later stage of fluid evolution and mineral precipitation in a hydrothermal fluid system. The present study therefore indicates that Zn of the Fusheng, Daliangzi, Maozu, Jinshachang, and Tianbaoshan deposits is predominantly derived from Sinian to lower Permian sedimentary rocks, while in the Tianbaoshan deposit minor Zn originates from Proterozoic folded basement beneath the Sinian Dengying Formation.

Implications for metal sources and pathways of ore-forming fluids

In combination with previously published Tianbaoshan data (+ 0.01 to + 0.57‰; Zhu et al. 2016), sphalerites from the Tianbaoshan, Fusheng, Daliangzi, Maozu, and Jinshachang deposits have δ^{114}Cd values of − 0.10 to + 0.57‰, consistent with the general range for sphalerites of Pb–Zn deposits in SW China (− 0.59 to + 0.57‰; Fig. 9). Zhu et al. (2013) indicated that Pb–Zn deposits with different origins are plotted within distinct fields in a 1/Cd–δ^{114}Cd diagram (Fig. 10a). Data for all samples from the present study plot in the MVT field (Fig. 10a), consistent with their geological characteristics (ESM 1). Furthermore, data for most samples from the five

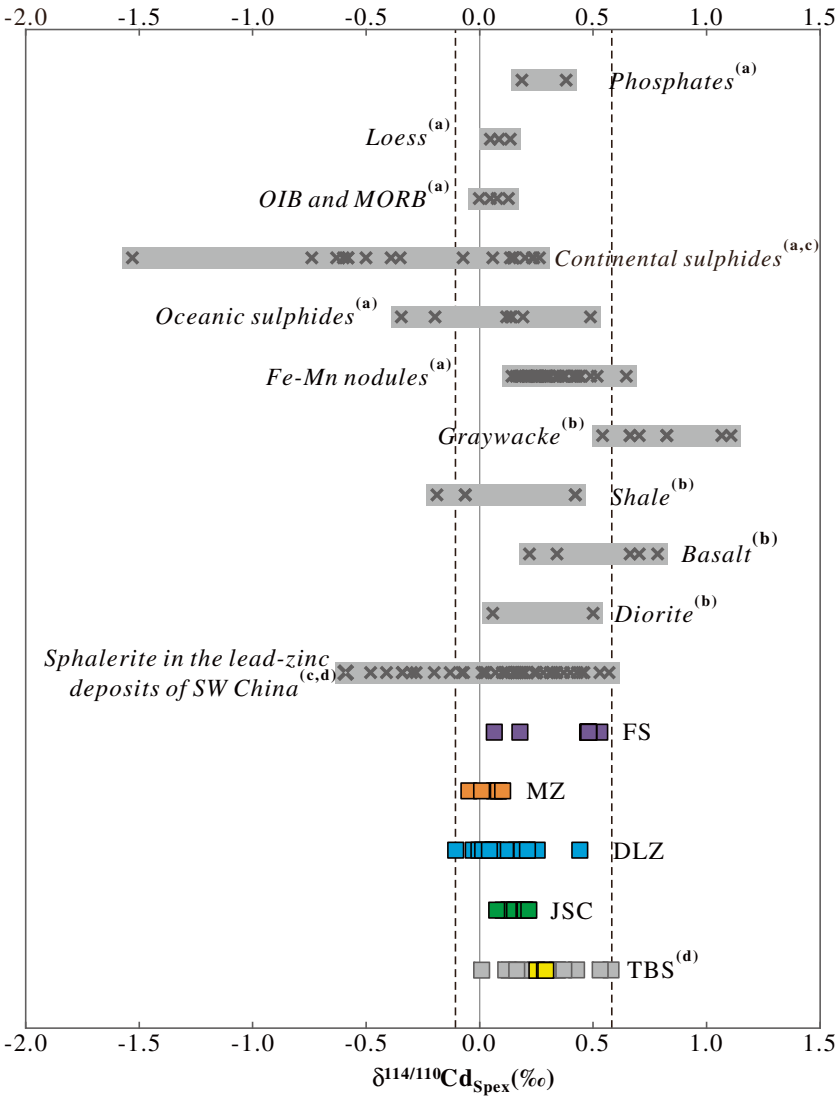

Fig. 9 Summary of Cd isotopic compositions of solid samples (After Zhu et al. 2015). Data sources: [a]Schmitt et al. 2009; [b]Wombacher et al. 2003; [c]Zhu et al. 2013; [d]Zhu et al. 2016

deposits plot within the low-temperature field as defined by Wen et al. (2016) (Fig. 10b), with Cd isotopic compositions and elemental ratios distinct from those of high-temperature systems such as porphyry, magmatic-hydrothermal, skarn, and volcanic massive sulfide (VMS) deposits and sedimentary exhalative systems (SEDEX deposits). This observation agrees well with the homogenization temperatures based on previous fluid inclusion studies and geological characteristics of these deposits (ESM 1). In conclusion, the sources, ore-forming fluid pathways, and metallogenic processes of the studied deposits are comparable with MVT Pb-Zn deposits.

The lack of correlation between $\delta^{66}Zn$ and $\delta^{34}S$ values of the Tianbaoshan, Fusheng, Daliangzi, and Maozu deposits (Fig. 11a) implies that Zn and S are derived from different fluids. Furthermore, the large variations in $\delta^{66}Zn$, but insignificant variations in $\delta^{34}S$ values, indicate rapid deposition of ores when Zn-bearing fluid reacted with S-bearing fluid. In contrast, Jinshachang deposit data can be grouped into lower and higher $\delta^{34}S$ values (Fig. 11a), implying that S originates from two sources: Proterozoic folded basement and sulfates coexisting with sulfides. The almost linear correlation between $\delta^{66}Zn$ and $\delta^{34}S$ values (Fig. 11a) in each of these Jinshachang groups may be explained by either long-distance

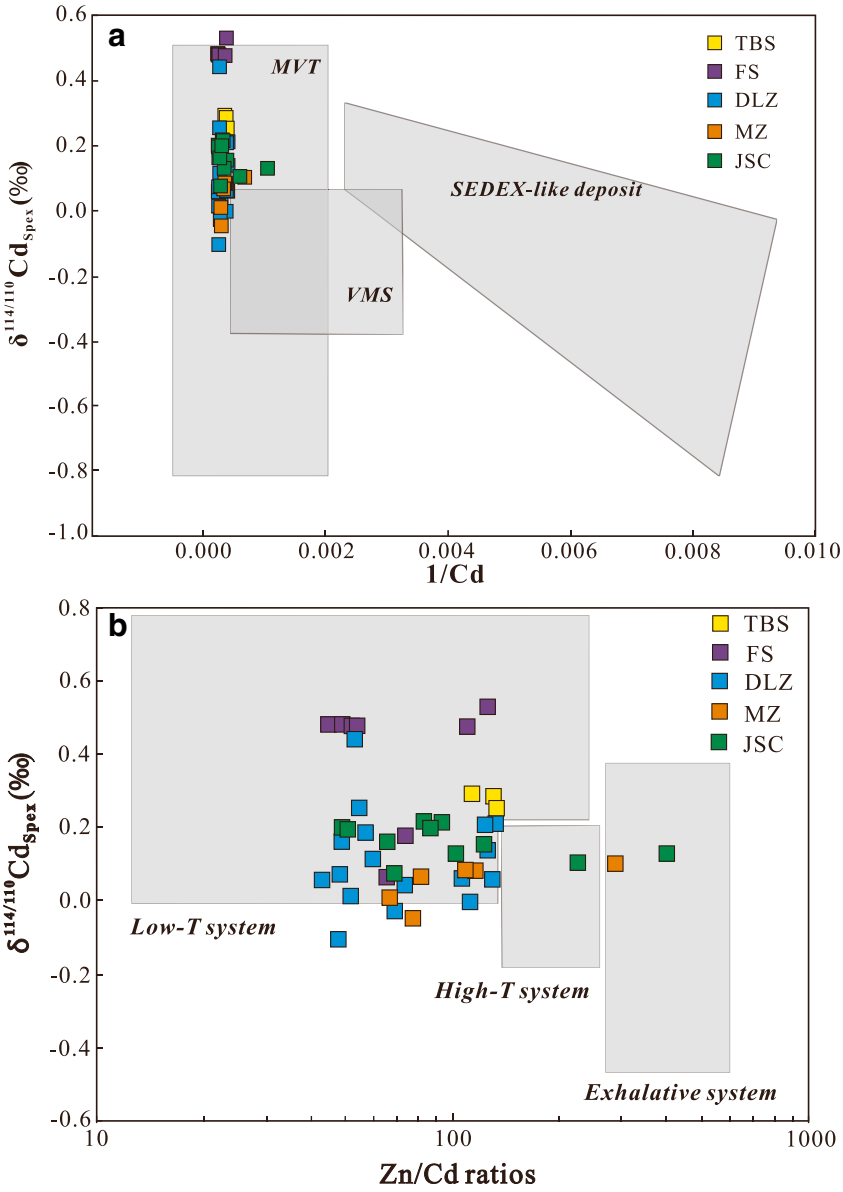

Fig. 10 **a** The Cd contents and isotopic compositions of the studied Pb-Zn deposits (after Zhu et al. 2013). **b** Distribution of Zn/Cd ratios versus Cd isotopic compositions of the studied Pb-Zn deposits (after Wen et al. 2016)

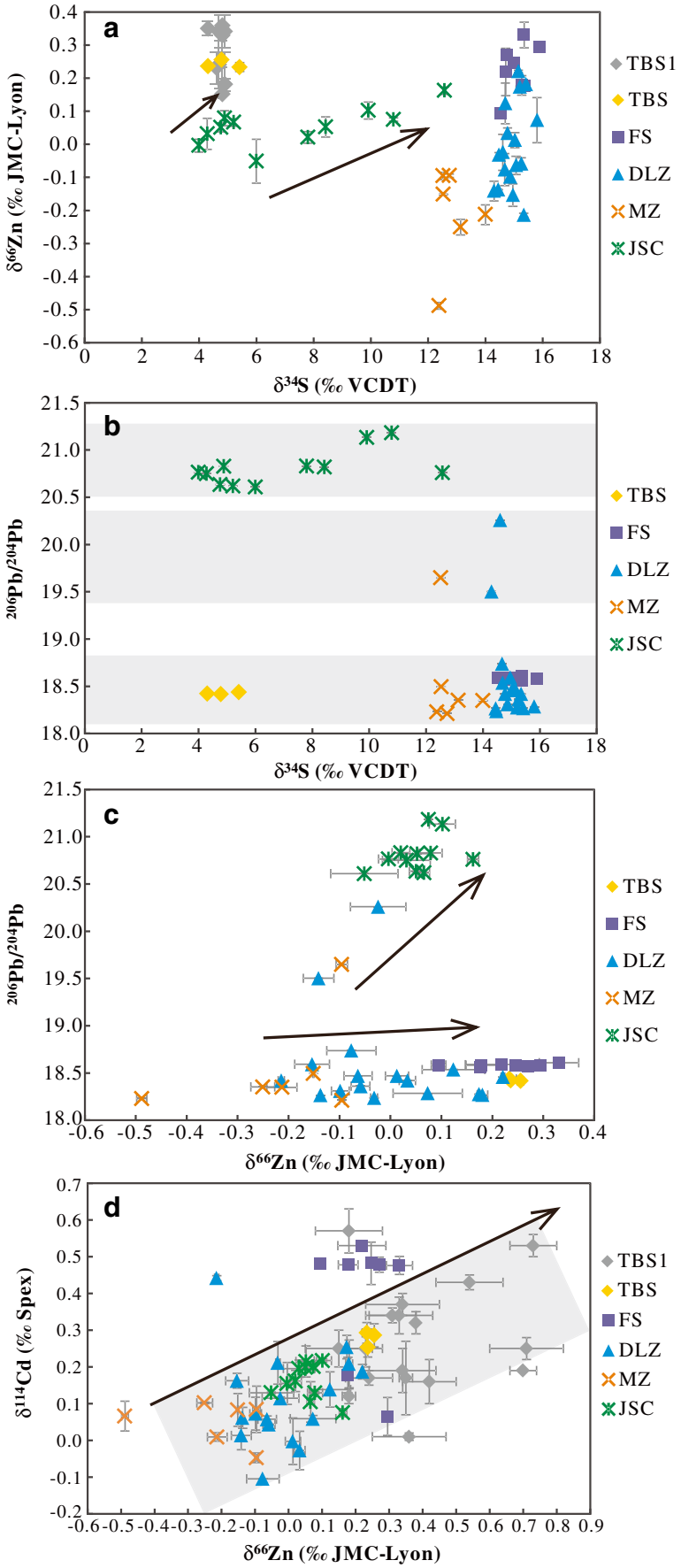

Fig. 11 **a** Zinc isotope compositions of sphalerite in the studied Pb-Zn deposits as a function of sulfur isotope compositions. **b** Lead isotope compositions of sphalerite in the studied Pb-Zn deposits as a function of sulfur isotope compositions. **c** Lead isotope compositions of sphalerite in the studied Pb-Zn deposits as a function of zinc isotope compositions. **d** Cadmium isotope compositions of sphalerite in the studied Pb-Zn deposits as a function of zinc isotope compositions. Data sources: TBS1 (He et al. 2016; Zhu et al. 2016)

migration of ore-forming fluid or long-period ore precipitation. Moreover, $^{206}Pb/^{204}Pb$ ratios exhibit no correlation with $\delta^{34}S$ values for all five deposits (Fig. 11b), possibly also due to mixing of Pb- and S-bearing fluids. At least two stratigraphic end-members provided Pb for the studied deposits: upper Sinian and Devonian to lower Permian sedimentary rocks with less radiogenic Pb, and Proterozoic basement and Cambrian sedimentary rocks with more radiogenic Pb (Fig. 11b). Furthermore, Pb of the Daliangzi and Maozu deposits likely originated from both these end-members, with upper Sinian and Devonian to lower Permian sedimentary rocks providing more Pb. The weak linear correlation between sphalerite $^{206}Pb/^{204}Pb$ ratios and $\delta^{66}Zn$ values (Fig. 11c) indicates that parts of Pb and Zn in the studied deposits may originate from the same source rocks, and the significant variations in $\delta^{66}Zn$ values (Fig. 11c) may be due to kinetic Raleigh fractionation during fluid evolution and mineral precipitation.

The weak positive correlation between $\delta^{114}Cd$ and $\delta^{66}Zn$ values (Fig. 11d) indicates that the isotopic fractionation mechanisms of Cd and Zn in hydrothermal systems could be similar as mentioned previously (i.e., the sources, temperature effects, and isotopic fractionation during fluid evolution and mineral precipitation). As a result, Zn and Cd isotopic compositions became heavier from Maozu to Daliangzi, Jinshachang, and Tianbaoshan (Fig. 11d). Ore-hosting strata of the four deposits are all of the upper Sinian Dengying Formation. If their ore-forming fluids were derived from the same hydrothermal fluid system, there would be a trend of enrichment in heavier Zn and Cd isotopes following the migration of fluids and precipitation of minerals. As illustrated in Fig. 1, there are several hundred Pb-Zn deposits of different size in the SYG area, and the distribution of the Pb–Zn deposits is controlled by several regional faults. These faults could be linked at depth to act as fluid pathways. Also, the ancient elevation for Maozu is the highest, assuming that these locations of Pb-Zn mineralization experienced similarly late-stage uplift. In combination of Cd and Zn isotopic fractionation characteristics presented in this study, we propose that the ore-forming fluids most likely flowed through Maozu first, then migrated along the Xiaojiang and Anninghe fault belts and their branch faults (Fig. 1), migrating to Daliangzi, Jinshachang, and Tianbaoshan, respectively. The lack of correlation between $\delta^{114}Cd$ and $\delta^{66}Zn$ values of the Fusheng deposit (Fig. 11d) could be explained by the addition of different hydrothermal fluids or the rapid precipitation of ores. Isotopically heavier Zn and Cd compositions could thus provide a geochemical fingerprint for detecting remote orebodies in large hydrothermal systems.

Based on the above considerations, we infer that the metallogenic processes involved in the studied Pb–Zn deposits are as follows. Tectonic events related to the Indosinian Orogeny and post-Late Triassic completion of suturing between the Indochina and South China blocks around the study area (Cai and Zhang 2009) led to the development of a series of thrust belts and foreland basins on the periphery of the SYG triangle. During diagenesis in these foreland basins, basinal brines formed from seawater or evaporative brines buried with sediments. Evaporative brines and dissolved halite provided the chloride (ESM 1) for metal complexation, while clastic basinal sediments and folded basement provided Zn, Pb, Fe, and other ore-forming metals (Wang et al. 2014). Orogenesis during the Late Triassic contributed to long-distance migration and accumulation of basin brines, driven by gravity and topography. The basin brines then migrated along major faults and associated fracture zones or karst systems into reactive carbonates, finally accumulating in different open areas. During this migration, the basin brines evolved into metal-bearing fluids through the extraction of ore-forming metals from upper Sinian and Devonian to lower Permian sedimentary rocks (Fusheng, Daliangzi, and Maozu) or Proterozoic folded basement (Tianbaoshan), while evaporative brines in host strata evolved into reduced S-bearing fluids through TSR. Some S in the Tianbaoshan and Jinshachang deposits is derived from Meso–Neoproterozoic folded basement beneath the Dengying Formation. Faults provided a connection for the mixing of metal-bearing and reduced S-bearing fluids, leading to precipitation of ore minerals and formation of deposits. The formation of the Jinshachang deposit may have involved long-distance migration of ore-forming fluid or a long period of ore precipitation, in contrast to the rapid precipitation of ores in the Fusheng deposit, possibly related to whether there was sufficient volume for ore deposition. Finally, the Pb–Zn ores were hosted in structural fractures, block fracture zones (Daliangzi deposit), and pre-ore carbonate dissolution caves (Fig. 4 F1), where the orebodies occur as open space fillings in breccias (Fig. 4 D2, M1) and fractures (Fig. 4 D1) or replacing host dolostone (Fig. 4 T1, T2), and display characteristics of epigenetic, stratabound (Fig. 4 F2), and carbonate-hosted sulfide bodies. The heat source for the ore-forming fluids could have been derived from abnormal geothermal gradients triggered by Late Triassic orogenesis during basin evolution.

Conclusions

This study of Pb–Zn–S–Cd isotopic compositions of sulfides (sphalerite and galena) in the Tianbaoshan, Fusheng, Daliangzi, Maozu, and Jinshachang Pb–Zn deposits has led to the following conclusions.

(1) Mixing of metal-bearing and reduced S-bearing fluids leads to precipitation of ore minerals and the formation of Pb-Zn deposits. Sulfur in the studied deposits is mainly derived from evaporates or seawater sulfates in Cambrian to Triassic sedimentary strata, Meso–Neoproterozoic folded basement, and sulfates coexisting with sulfides. At least two stratigraphic end-members provide Pb and Zn for the studied deposits, i.e., upper Sinian and Devonian to lower Permian sedimentary rocks with less radiogenic Pb, and Proterozoic basement and Cambrian sedimentary rocks with more radiogenic Pb.
(2) It is proposed that the ore-forming fluids of the Tianbaoshan, Daliangzi, Maozu, and Jinshachang deposits came from the same hydrothermal fluid system. The ore-forming fluids most likely flowed through Maozu first, then migrated along the Xiaojiang and Anninghe fault belts and their branch faults, to Daliangzi, Jinshachang, and Tianbaoshan, respectively.
(3) Zn and Cd isotopic compositions could be useful tools in tracing pathways of ore-forming fluids in Pb–Zn deposits, and isotopically heavier Zn and Cd compositions could provide a geochemical fingerprint for detecting remote orebodies in large hydrothermal fluid systems.

Acknowledgements Yubo Li, Lianzhong Qi, and Bo Zheng are thanked for the help in field work. We appreciated the constructive comments and suggestions from Ryan Mathur and an anonymous reviewer, and the handling of Prof. Bernd Lehmann, which significantly improve the quality of this paper.

Funding information This research is jointly supported by the National Basic Research Program of China (2014CB440903) and the National Science Foundation of China (41425011).

References

Abouchami W, Galer SJG, Horner TJ, Rehkämper M, Wombacher F, Xue ZC, Lambelet M, Gault-Ringold M, Stirling CH, Schönbächler M, Shiel AE, Weis D, Holdship PF (2012) A common reference material for cadmium isotope studies – NIST SRM 3108. Geostand Geoanal Res 37:5–17

Albarède F (2004) The stable isotope geochemistry of copper and zinc. Rev Mineral Geochem 55:409–427

Bai JH, Huang ZL, Zhu D, Yan ZF, Zhou JX (2013) Isotopic compositions of sulfur in the Jinshachang lead–zinc deposit, Yunnan, China. Acta Geol Sin Engl 87:1355–1369

Basuki NI, Taylor BE, Spooner ETC (2008) Sulfur isotope evidence for thermochemical reduction of dissolved sulfate in Mississippi Valley type zinc–lead mineralization, Bongara area, northern Peru. Econ Geol 103:183–799

Belshaw NS, Freedman PA, O'Nions RK, Frank M, Guo Y (1998) A new variable dispersion double–focusing plasma mass spectrometer with performance illustrated for Pb isotopes. Int J Mass Spectrom 181: 51–58

Bentahila Y, Othman DB, Luck JM (2008) Strontium, lead and zinc isotopes in marine cores as tracers of sedimentary provenance: a case study around Taiwan orogen. Chem Geol 248:62–82

Borrok DM, Wanty RB, Ridley WI, Wolf R, Lamothe PJ, Adams M (2007) Separation of copper, iron, and zinc from complex aqueous solutions for isotopic measurement. Chem Geol 242:400–414

Cai JX, Zhang KJ (2009) A new model for the Indochina and South China collision during the Late Permian to the Middle Triassic. Tectonophys 467:35–43

Chen H, Savage PS, Teng FZ, Helz RT, Moynier F (2013) Zinc isotope fractionation during magmatic differentiation and the isotopic composition of the bulk earth. Earth Planet Sci Lett 369:34–42, 369-370

Chen SJ (1986) Research on the genesis of lead–zinc ore–deposits in western Guizhou and northeastern Yunnan. Guizhou Geol 3:211–222 in Chinese with English abstract

Claypool GE, Holser WT, Kaplan IR, Sakai H, Zak I (1980) The age curves of sulfur and oxygen isotopes in marine sulfate and their mutual interpretation. Chem Geol 28:199–260

Clayton RN (1981) Isotopic thermometry. In: Newton RC et al (eds) Thermodynamics of minerals and melts. Speinger Verlag, New York, pp 85–109

Dauphas N, Pourmand A, Teng FZ (2009) Routine isotopic analysis of iron by HR–MC–ICPMS: how precise and how accurate? Chem Geol 267:175–184

Dekov VM, Cuadros J, Kamenov GD (2010) Metalliferous sediments from the HMS challenger voyage (1872–1876). Geochim Cosmochim Acta 74:5019–5038

Duan JL, Tang JX, Lin B (2016) Zinc and lead isotope signatures of the Zhaxikang Pb–Zn deposit, South Tibet: implications for the source of the ore–forming metals. Ore Geol Rev 78:58–68

Fernandez A, Borrok DM (2009) Fractionation of Cu, Fe, and Zn isotopes during the oxidative weathering of sulfide-rich rocks. Chem Geol 264:1–12

Fu SH (2004) Metallogenesis of Pb–Zn deposits and enrichment regularity of dispersed elements Cd, Ga and Ge in SW Yangtze block. PhD thesis, Chengdu University of Science and Technology, Chengdu, China, pp 1-66 (in Chinese with English abstract)

Gagnevin D, Boyce AJ, Barrie CD, Menuge JF, Blakeman RJ (2012) Zn, Fe and S isotope fractionation in a large hydrothermal system. Geochim Cosmochim Acta 88:183–198

Gao S, Yang J, Zhou L, Li M, Hu ZC, Guo JL, Yuan HL, Gong HJ, Xiao GQ, Wei JQ (2011) Age and growth of the Archean Kongling terrain, South China, with emphasis on 3.3 Ga granitoid gneisses. Am J Sci 311:153–182

Gao ZF, Zhu XK, Sun J, Luo ZH, Bao C, Tang C, Ma JX (2018) Spatial evolution of Zn–Fe–Pb isotopes of sphalerite within a single ore body: a case study from the Dongshengmiao ore deposit, Inner Mongolia, China. Mineral Deposita 53:55–65

Guan SP, Li ZX (1999) Lead–sulfur isotope study of carbonate–hosted lead–zinc deposits at eastern margin of the Kangdian axis. Geol Geochem 27:45–54 in Chinese with English abstract

Guo X (2007) Ore–forming characteristics of the Jinshachang Pb–Zn deposit and the perspective prediction of its deep part and periphery, Northeast Yunnan. Miner. Resour Geol 21:636–641 in Chinese with English abstract

Han RS, Hu YZ, Wang XK, Hou BH, Huang ZL, Chen J, Wang F, Wu P, Li B, Wang HJ, Dong Y, Lei L (2012) Mineralization model of rich Ge–Ag–bearing Zn–Pb polymetallic deposit concentrated district in northeastern Yunnan, China. Acta Geol Sin 86:280–294 in Chinese with English abstract

Han RS, Liu CQ, Huang ZL, Chen J, Ma DY, Lei L, Ma GS (2007a) Geological features and origin of the Huize carbonate–hosted Zn–Pb–(Ag) District, Yunnan, South China. Ore Geol Rev 31:360–383

Han RS, Zou HJ, Hu B, Hu YZ, Xue CD (2007b) Features of fluid inclusions and sources of ore–forming fluid in the Maoping carbonate–hosted Zn–Pb–(Ag–Ge) deposit, Yunnan, China. Acta Petrol Sin 23:2109–2118

He B, Xu YG, Huang XL, Luo ZY, Shi YR, Yang QJ, Yu SY (2007) Age and duration of the Emeishan flood volcanism, SW China: geochemistry and SHRIMP zircon U–Pb dating of silicic ignimbrites, post–volcanic Xuanwei formation and clay tuff at the Chaotian section. Earth Planet Sci Lett 255:306–323

He CZ, Xiao CY, Wen HJ, Zhou T, Zhu CW, Fan HF (2016) Zn–S isotopic compositions of the Tianbaoshan carbonate hosted Pb–Zn deposit in Sichuan, China: implications for source of ore components. Acta Petrol Sin 32:3394–3406 (in Chinese with English abstract)

He CZ (2017) Zinc-sulfur isotopic compositions of the Tianbaoshan carbonate-hosted Pb-Zn deposit in Sichuan, China: implications for source of ore components. Master thesis, Chinese Academy of Sciences, Guiyang, pp 1-65 (in Chinese with English abstract)

Hu RZ, Chen WT, Xu DR, Zhou MF (2017a) Reviews and new metallogenic models of mineral deposits in South China: an introduction. J Asian Earth Sci 137:1–8

Hu RZ, Fu SL, Huang YH, Zhou MF, Fu SH, Zhao CH, Wang YJ, Bi XW, Xiao JF (2017b) The giant South China Mesozoic low-temperature metallogenic domain: reviews and a new geodynamic model. J Asian Earth Sci 137:9–34

Hu RZ, Fu SL, Xiao JF (2016) Major scientific problems on low–temperature metallogenesis in South China. Acta Petrol Sin 32: 3239–3251 in Chinese with English abstract

Hu RZ, Zhou MF (2012) Multiple Mesozoic mineralization events in South China–an introduction to the thematic issue. Mineral Deposita 47:579–588

Hu YG (1999) Ag occurrence, source of ore–forming metals and mechanism of Yinchangpo Ag–Pb–Zn deposit. PhD thesis, Chinese Academy of Sciences, Guiyang, pp 2-45 (in Chinese with English abstract)

Huang CJ, Li ZQ, Wang JZ (2015) Pb isotopic features of the Lala IOCG ore deposit on the southwestern margin of the Yangtze Block and their significance. Geol Bull China 34:501–507 in Chinese with English abstract

Huang J, Liu SA, Gao YJ, Xiao YL, Chen S (2016) Copper and zinc isotope systematics of altered oceanic crust at IODP Site 1256 in the eastern equatorial Pacific. J Geophys Res 121:7086–7100

Huang ZL, Chen J, Han RS, Li WB, Liu CQ, Zhang ZL, Ma DY, Gao DR, Yang HL (2004) Geochemistry and ore–formation of the Huize Giant lead–zinc deposit, Yunnan Province, China: discussion on the relationship between Emeishan flood basalts and lead–zinc mineralization. Geological Publishing House, Beijing, pp 28–30 (in Chinese)

Huang ZL, Li WB, Chen J, Han RS, Liu CQ, Xu C, Guan T (2003) Carbon and oxygen isotope constraints on the mantle fluids join the mineralization of the Huize super–large Pb–Zn deposits, Yunnan Province. China J Geochem Explor 78:637–642

Jiang SY, Lu JJ, Gu LX, Hua RM, Jiang YH (2001) Determination of Cu, Zn, Fe isotopic compositions by MC–ICPMS and their geological applications. Bull Mineral Petrol Geochem 4:431–433 in Chinese with English abstract

John S, Rouxel O, Craddock P, Engwall A, Boyle E (2008) Zinc stable isotopes in seafloor hydrothermal vent fluids and chimneys. Earth Planet Sci Lett 269:17–28

Kelley KD, Wilkinson JJ, Chapman JB, Crowther HL, Weiss DJ (2009) Zinc isotopes in sphalerite from base metal deposits in the Red Dog district, Northern Alaska. Econ Geol 104:767–773

Kou LL, Zhang S, Zhong KH (2015) Geochemical differences between Daliangzi and Tianbaoshan lead–zinc deposits in huili–huidong area, Sichuan, China: tectonic implication. Geol Resour 24:26–32 in Chinese with English abstract

Kunzmann M, Halverson GP, Sossi PA, Raub TD, Payne JL, Kirby J (2013) Zn isotope evidence for immediate resumption of primary productivity after snowball earth. Geol 41:27–30

Li FY (2003) Study on occurrence state and enrichment mechanism of dispersed elements in MVT deposits: a case study for the Tianbaoshan and Daliangzi Pb–Zn deposits in Sichuan Province. MSc thesis, Chengdu University of Science and Technology, Chengdu, China, pp 1-69 (in Chinese with English abstract)

Li SZ, Zhu XK, Tang SH, He XX, Cai JJ (2008) The application of MC-ICP-MS to high-precision measurement of Zn isotope ratios. Acta Petrol Mineral 27:273–278 in Chinese with English abstract

Li WB, Huang ZL, Yin MD (2007) Isotope geochemistry of the Huize Zn–Pb ore field, Yunnan Province, Southwestern China: implication for the sources of ore fluid and metals. Geochem 41:65–81

Li X, Wang J, Chu F, Lei J, Wang H, Li Z (2017) Zn isotopes in hydrothermal sulfides and their oxidation products along the south mid–Atlantic ridge: evidence of hydrothermal fluid deposition. Geo-Mar Lett:1–8

Little SH, Vance D, McManus J, Severmann S (2016) Key role of continental margin sediments in the oceanic mass balance of Zn and Zn isotopes. Geol 44:207–210

Little SH, Vance D, Walker–Brown C, Landing WM (2014) The oceanic mass balance of copper and zinc isotopes, investigated by analysis of their inputs, and outputs to ferromanganese oxide sediments. Geochim Cosmochim Acta 125:673–693

Liu WZ (2009) Geological and geochemical characteristics and metallogenic mechanism analysis of the Pb–Zn deposit in Maozu, Yunnan, China. J Chengdu Univ Technol 36:480–486 (in Chinese with English abstract)

Liu HC, Lin WD (1999) Study on the law of Pb–Zn–Ag ore deposits in Northeast Yunnan, China. Yunnan University Press, Kunming, pp 1–468 (in Chinese)

Liu WH, Zhang J, Wang J (2017) Sulfur isotope analysis of carbonate-hosted Zn–Pb deposits in northwestern Guizhou Province, Southwest China: implications for the source of reduced sulfur. J Geochem Explor 181:31–44

Lv YW, Liu SA, Zhu JM, Li SG (2016) Copper and zinc isotope fractionation during deposition and weathering of highly metalliferous black shales in Central China. Chem Geol 422:82–93

Maréchal CN, Nicolas E, Douchet C, Albarède F (2000) Abundance of zinc isotopes as a marine biogeochemical tracer. Geochem Geophys Geosyst 1(5)

Maréchal CN, Télouk P, Albarède F (1999) Precise analysis of copper and zinc isotopic compositions by plasma–source mass spectrometry. Chem Geol 156:251–273

Mason TF, Weiss DJ, Chapman JB, Wilkinson JJ, Tessalina SG, Spiro B, Horstwood MS, Spratt J, Coles BJ (2005) Zn and Cu isotopic variability in the Alexand rinka volcanic–hosted massive sulfide (VHMS) ore deposit, Urals, Russia. Chem Geol 221:170–187

Ohmoto H (1972) Systematics of sulfur and carbon isotopes in hydrothermal ore deposits. Econ Geol 67:551–579

Ohmoto H, Goldhaber MB (1997) Sulfur and carbon isotopes. In: Barnes HL (ed) Geochemistry of hydrothermal ore deposits, third ed. Wiley, New York, pp 517–611

Ohmoto H, Rye RO (1979) Isotopes of sulfur and carbon. In: Geochemistry of hydrothermal ore deposits, pp 509–567

Ohmoto HIROSHI, Kaiser CJ, Geer KA (1990) Systematics of sulphur isotopes in recent marine sediments and ancient sediment–hosted base metal deposits. Stable isotopes and fluid processes in mineralization, vol 23. Geology Department and Extension Service, University of Western Australia, pp 70–120

Pašava J, Tornos F, Chrastný V (2014) Zinc and sulfur isotope variation in sphalerite from carbonate-hosted zinc deposits, Cantabria, Spain. Mineral Deposita 49:797–807

Pichat S, Douchet C, Albarède F (2003) Zinc isotope variations in deep–sea carbonates from the eastern equatorial Pacific over the last 175 ka. Earth Planet Sci Lett 210:167–178

Qiu YM, Gao S, McNaughton NJ, Groves DI, Ling WL (2000) First evidence of > 3.2 Ga continental crust in the Yangtze craton of South China and its implications for Archean crustal evolution and Phanerozoic tectonics. Geol 28:11–14

Robinson BW, Kusakabe M (1975) Quantitative preparation of sulfur dioxide for $^{32}S/^{34}S$ analyses from sulfides by combustion with cuprous oxide. Anal Chem 47:1179–1181

Schmitt AD, Stephen JG, Abouchami W (2009) Mass–dependent cadmium isotopic variations in nature with emphasis on the marine environment. Earth Planet Sci Lett 277:262–272

Schoenberg R, Von BF (2005) An assessment of the accuracy of stable Fe isotope ratio measurements on samples with organic and inorganic matrices by high–resolution multicollector ICP–MS. Int J Mass Spectrom 242:257–272

Schwartz MO (2000) Cadmium in zinc deposits: economic geology of a polluting element. Int Geol Rev 42:445–469

Seal RR (2006) Sulfur isotope geochemistry of sulfide minerals. Rev Mineral Geochem 61:633–677

Shao SC, Li CY (1997) The geochemical constrains on genesis of stratabound Pb–Zn deposits in Dengying formation at western margin of Yangtze platform. Bull Mineral Petrol Geochem 16:30–33 in Chinese with English abstract

Si RJ (2005) Ore deposit geochemistry of the Fule dispersed element–polymetallic deposit, Yunnan Province. PhD thesis, Chinese Academy of Sciences, Guiyang, China, pp 1–131 (in Chinese with English abstract)

Sivry Y, Riotte J, Sonke J, Audry S, Schäfer J, Viers J, Blanc G, Freydier R, Dupré B (2008) Zn isotopes as tracers of anthropogenic pollution from Zn–ore smelters the Riou Mort–Lot river system. Chem Geol 255:295–304

Tang SH, Zhu XK, Li J, Yan B, Li SZ, Li ZH, Wang Y, Sun J (2016) New standard solutions for measurement of Iron, copper and zinc isotopic compositions by multi–collector inductively coupled plasma–mass spectrometry. Rock Miner Anal 35:127–133 in Chinese with English abstract

Toutain JP, Sonke J, Munoz M, Nonell A, Polvé M, Viers J, Freydier R, Sortino F, Joron JL, Sumarti S (2008) Evidence for Zn isotopic fractionation at Merapi volcano. Chem Geol 253:74–82

Tu GC (1984) Geochemistry of strata–bound ore deposits in China. Science Press, Beijing, pp 13–69 in Chinese

Tu GC, Gao ZM, Hu RZ, Zhang Q, Li CY, Zhao ZH, Zhang BG (2004) The geochemistry and deposit-forming mechanism of disperse element. Geological Publishing House, Beijing, pp 1–153 in Chinese

Wang CM, Deng J, Carranza EJM, Lai XR (2014) Nature, diversity and temporal–spatial distributions of sediment-hosted Pb—Zn deposits in China. Ore Geol Rev 56:327–351

Wang XC, Zheng ZR, Zheng MH, Xu XH (2000) Metallogenic mechanism of the Tianbaoshan Pb–Zn deposit. Sichuan Chin J Geochem 19:121–133

Weiss DJ, Rausch N, Mason TFD, Coles BJ, Wilkinson JJ, Ukonmaanaho L, Arnold T, Nieminen TM (2007) Atmospheric deposition and isotope biogeochemistry of zinc in ombrotrophic peat. Geochim Cosmochim Acta 71:3498–3517

Wen HJ, Zhu CW, Zhang YX, Cloquet C, Fan HF, Fu SH (2016) Zn/Cd ratios and cadmium isotope evidence for the classification of lead–zinc deposits. Sci Rep 6:25273

Wilkinson JJ, Weiss DJ, Mason TFD, Coles BJ (2005) Zinc isotope variation in hydrothermal systems: preliminary evidence from the Irish Midlands ore field. Econ Geol 100:583–590

Wombacher F, Rehkämper M, Mezger K (2004) Determination of the mass–dependence of cadmium isotope fractionation during evaporation. Geochim Cosmochim Acta 68:2349–2357

Wombacher F, Rehkämper M, Mezger K, Münker C (2003) Stable isotope compositions of cadmium in geological materials and meteorites determined by multiple–collector ICP–MS. Geochim Cosmochim Acta 67:4639–4654

Wu Y (2013) The age and ore–forming process of MVT deposits in the boundary area of Sichuan–Yunnan–Guizhou provinces, Southwest China. PhD thesis, China University of Geoscience, Beijing, China, pp 1–175 (in Chinese with English abstract)

Wu Y, Zhang CQ, Mao JW, Ouyang HG, Sun J (2013) The genetic relationship between hydrocarbon systems and Mississippi Valley–type Zn–Pb deposits along the SW margin of Sichuan Basin, China. Int Geol Rev 55:941–957

Xie JR (1941) Introduction to ore deposits in Yunnan Province. Geol Rev 6:1–42 in Chinese

Xie JR (1963) Introduction of the Chinese ore deposits. Scientific Books Publishing House, Beijing, pp 1–71 in Chinese

Xu YG, Luo ZY, Huang XL, He B, Xiao L, Xie LW, Shi YR (2008) Zircon U–Pb and Hf isotope constraints on crustal melting associated with the Emeishan mantle plume. Geochim Cosmochim Acta 72:3084–3104

Yan ZF, Huang ZL, Xu C, Chen M, Zhang ZL (2007) Signatures of the source for the Emeishan flood basalts in the Ertan area: Pb isotope evidence. Chin J Geochem 26:207–213

Yang JL, Li YB, Liu SQ, Tian HQ, Chen CY, Liu JM, Shi YL (2015) Theoretical calculations of Cd isotope fractionation in hydrothermal fluids. Chem Geol 391:74–82

Ye L, Nigel JK, Cristiana LC, Liu YP, Zhang Q, Liu TG, Gao W, Yang YL, Leonid D (2011) Trace and minor elements in sphalerite from base metal deposits in South China: a LA–ICPMS study. Ore Geol Rev 39:188–217

Yu L (2014) Brief study on the fluid inclusion characteristics and its genetic significance of Tianbaoshan Pb–Zn deposit in Huili County, Sichuan Province. MSc Thesis, Chengdu University of Science and Technology, Chengdu, China, pp 1–67 (in Chinese with English abstract)

Yuan B, Mao JW, Yan XH, Wu Y, Zhang F, Zhao LL (2014) Sources of metallogenic materials and metallogenic mechanism of Daliangzi ore field in Sichuan Province: constraints from geochemistry of S, C, H, O, Sr isotope and trace element in sphalerite. Acta Petrol Sin 30:209–220 in Chinese with English abstract

Zhang CQ (2008) The genetic model of Mississippi Valley–type deposits in the boundary area of Sichuan, Yunnan and Guizhou Province, China. PhD thesis, Chinese Academy of Geological Sciences, Beijing, China, pp 1–177 (in Chinese with English abstract)

Zhang CQ, Mao JW, Yu JJ, Li HM (2007) Study on fluid inclusion and the metallogenetic mechanism of Chipu Pb–Zn deposit in Sichuan, China. Acta Petrol Sin 23:2541–2552 in Chinese with English abstract

Zhang CQ, Rui ZY, Chen YC, Wang DH, Chen ZH, Luo DB (2013) The main successive strategic bases of resources for Pb–Zn deposits in China. Geol China 40:248–272 in Chinese with English abstract

Zhang CQ, Wu Y, Hou L, Mao JW (2015) Geodynamic setting of mineralization of Mississippi Valley–type deposits in world–class Sichuan–Yunnan–Guizhou Zn–Pb triangle, Southwest China: implications from age–dating studies in the past decade and the Sm–Nd age of Jinshachang deposit. J Asian Earth Sci 103:103–114

Zhang QH, Mao JQ, Guang SY (1998) The studies of ore–forming material sources of metal deposit in Hezhang Pb–Zn mine, Shuicheng, Guizhou province. J Guizhou Univ Technol 27:26–34 in Chinese with English abstract

Zhang WJ (1984) A preliminary discussion on the sedimentary origin and metallogenic rule of Pb–Zn deposits in northeastern Yunnan. J Geol Explorat 7:11–16 in Chinese with English abstract

Zhang YX, Wen HJ, Zhu CW, Fan HF, Luo CG, Liu J, Cloquet C (2016) Cd isotope fractionation during simulated and natural weathering. Environ Pollut 216:9–17

Zhao XF, Zhou MF, Li JW, Sun M, Gao JF, Sun WH, Yang JH (2010) Late Paleoproterozoic to early Mesoproterozoic Dongchuan Group in Yunnan, SW China: implications for tectonic evolution of the Yangtze Block. Precambrian Res 182:57–69

Zhao Y, Vance D, Abouchami W, De BHJW (2014) Biogeochemical cycling of zinc and its isotopes in the Southern Ocean. Geochim Cosmochim Acta 125:653–672

Zhao Z (1995) Metallogenic model of Pb–Zn deposits in northeastern Yunnan. J Yunnan Geol 14:350–354 in Chinese with English abstract

Zheng MH, Wang XC (1991) Genesis of the Daliangzi Pb–Zn deposit in Sichuan, China. Econ Geol 86:831–846

Zhong H, Zhu W-G (2006) Geochronology of layered mafic intrusions from the pan–xi area in the Emeishan large igneous province, SW China. Mineral Deposita 41:599–606

Zhong H, Campbell IH, Zhu W-G, Allen CM, Hu R-Z, Xie L-W, He D-F (2011) Timing and source constraints on the relationship between mafic and felsic intrusions in the Emeishan large igneous province. Geochim Cosmochim Acta 75:1374–1395

Zhou CX, Wei SS, Guo JY, Li CY (2001) The source of metals in the Qilinchang Zn–Pb deposit, northeastern Yunnan, China: Pb–Sr isotope constrains. Econ Geol 96:583–598

Zhou JX, Bai JH, Huang ZL, Zhu D, Yan ZF, Lv ZC (2015) Geology, isotope geochemistry and geochronology of the Jinshachang carbonate–hosted Pb–Zn deposit, Southwest China. J Asian Earth Sci 98:272–284

Zhou JX, Gao JG, Chen D, Liu XK (2013a) Ore genesis of the Tianbaoshan carbonate hosted Pb–Zn deposit, Southwest China: geologic and isotopic (C–H–O–S–Pb) evidence. Int Geol Rev 55: 1300–1310

Zhou JX, Huang ZL, Bao GP (2013b) Geological and sulfur–lead–strontium isotopic studies of the Shaojiwan Pb–Zn deposit, Southwest China: implications for the origin of hydrothermal fluids. J Geochem Explor 128:51–61

Zhou JX, Huang ZL, Gao JG, Yan ZF (2013c) Geological and C–O–S–Pb–Sr isotopic constraints on the origin of the Qingshan carbonate–hosted Pb–Zn deposit, SW China. Int Geol Rev 55:904–916

Zhou JX, Huang ZL, Lv ZC, Zhu XK, Gao JG (2014a) Geology, isotope geochemistry and ore genesis of the Shanshulin carbonate–hosted Pb–Zn deposit, Southwest China. Ore Geol Rev 63:209–225

Zhou JX, Huang ZL, Yan ZF (2013d) The origin of the Maozu carbonate–hosted Pb–Zn deposit, Southwest China: constrained by C–O–S–Pb isotopic compositions and Sm–Nd isotopic age. J Asian Earth Sci 73:39–47

Zhou JX, Huang ZL, Zhou GF, Li XB, Ding W, Bao GP (2011) Trace elements and rare earth elements of sulfide minerals in the Tianqiao Pb–Zn ore deposit, Guizhou province, China. Acta Geol Sin Engl 85:189–199

Zhou JX, Huang ZL, Zhou MF, Li XB, Jin ZG (2013e) Constraints of C–O–S–Pb isotope compositions and Rb–Sr isotopic age on the origin of the Tianqiao carbonate–hosted Pb–Zn deposit, SW China. Ore Geol Rev 53:77–92

Zhou JX, Huang ZL, Zhou MF, Zhu XK, Muchez P (2014b) Zinc, sulfur and lead isotopic variations in carbonate–hosted Pb–Zn sulfide deposits, Southwest China. Ore Geol Rev 58:41–54

Zhou JX, Luo K, Li B, Huang ZL, Yan ZF (2016) Geological and isotopic constraints on the origin of the Anle carbonate–hosted Zn–Pb deposit in northwestern Yunnan Province, SW China. Ore Geol Rev 74:88–100

Zhou MF, Malpas J, Song XY, Robinson PT, Sun M, Kennedy AK, Lesher CM, Keays RR (2002) A temporal link between the Emeishan large igneous province (SW China) and the end–Guadalupian mass extinction. Earth Planet Sci Lett 196:113–122

Zhu CW (2014) Geochemistry of Cd and Ge, and their isotope in carbonate–hosted lead–zinc ore deposits in the boundary area of Sichuan, Yunnan and Guizhou provinces, China. PhD thesis, Chinese Academy of Sciences, Guiyang, China, pp 10–40 (in Chinese with English abstract)

Zhu CW, Liao SL, Wang W, Zhang YX, Yang T, Fan HF, Wen HJ (2018) Variations in Zn and S isotope chemistry of sedimentary sphalerite, Wusihe Zn-Pb deposit, Sichuan Province, China. Ore Geol Rev 95: 639–648

Zhu CW, Wen HJ, Zhang YX, Fan HF (2016) Cadmium and sulfur isotopic compositions of the Tianbaoshan Zn–Pb–Cd deposit, Sichuan Province, China. Ore Geol Rev 76:152–162

Zhu CW, Wen HJ, Zhang YX, Fan HF, Fu SH, Xu J, Qin TR (2013) Characteristics of Cd isotopic compositions and their genetic significance in the lead–zinc deposits of SW China. Sci China Earth Sci 56:2056–2065

Zhu CW, Wen HJ, Zhang YX, Fu SH, Fan HF, Cloquet C (2017) Cadmium isotope fractionation in the Fule Mississippi Valley–type deposit, Southwest China. Mineral Deposita 52:675–686

Zhu CW, Wen HJ, Zhang YX, Liu YZ, Wei RF (2015) Isotopic geochemistry of cadmium: a review. Acta Geol Sin Engl 89:2048–2057

Zhu XK, Guo Y, Williams RJP, O'Nions RK, Matthews A, Belshaw NS, Canters GW, De WEC, Weser U, Burgess BK, Salvato B (2002) Mass fractionation processes of transition metal isotopes. Earth Planet Sci Lett 200:47–62